

# Small System Collectivity in Relativistic Hadronic and Nuclear Collisions

James L. Nagle<sup>1</sup> and William A. Zajc<sup>2</sup>

<sup>1</sup>Department of Physics, University of Colorado, Boulder, Colorado 80309, USA; email: jamie.nagle@colorado.edu

<sup>2</sup>Department of Physics, Columbia University, New York, NY 10027, USA; email: waz1@columbia.edu

Annu. Rev. Nucl. Part. Sci. 2018. 68:1–36

This article's doi:  
10.1146/annurev-nucl-101916-123209

Copyright © 2018 by Annual Reviews.  
All rights reserved

## Keywords

QCD, RHIC, LHC, heavy ion collisions, quark–gluon plasma, QGP, relativistic hydrodynamics, perfect liquid, shear viscosity, relativistic fluid dynamics, gauge/gravity duality

## Abstract

The bulk motion of nuclear matter at the ultrahigh temperatures created in heavy ion collisions at the Relativistic Heavy Ion Collider and the Large Hadron Collider is well described in terms of nearly inviscid hydrodynamics, thereby establishing this system of quarks and gluons as the most perfect fluid in nature. A revolution in the field is under way, spearheaded by the discovery of similar collective, fluid-like phenomena in much smaller systems including  $p + p$ ,  $p + A$ ,  $d + \text{Au}$ , and  $^3\text{He} + \text{Au}$  collisions. We review these exciting new observations and their profound implications for hydrodynamic descriptions of small and/or out-of-equilibrium systems.

## Contents

1. INTRODUCTION .....	3
2. HISTORICAL PRELUDES .....	3
3. STANDARD MODEL OF HEAVY ION COLLISIONS .....	5
4. SMALL SYSTEM EXPERIMENTAL DATA .....	7
4.1. Two-Particle Correlations and Initial Observations .....	8
4.2. Instructive Measurements .....	10
4.3. Limits of Small System Flow Behavior .....	13
5. ADDITIONAL CONSIDERATIONS .....	16
5.1. Jet Quenching in Small Collision Systems? .....	16
5.2. Initial Conditions .....	18
5.3. Parton Transport Models .....	19
5.4. Momentum Correlations Explanations .....	21
6. HYDRODYNAMIC DISCUSSION AND IMPLICATIONS .....	22
7. SUMMARY .....	25

## 1. INTRODUCTION

The modern era of heavy ion physics began in the year 2000, with the first data taking at the Relativistic Heavy Ion Collider (RHIC), followed by heavy ion running at the Large Hadron Collider (LHC) in 2010. Shortly thereafter, a new arena for studying high-temperature nuclear matter came to the fore with a host of observations in small collision systems, including  $p + p$  and  $p(d, {}^3\text{He})+A$  collisions. These smaller systems exhibited many of the features of collective behavior found in collisions of heavy nuclei attributed to the perfect liquid nature of quark-gluon plasma<sup>1</sup> (QGP). While these observations were contrary to expectations, there is a long history of considering even small collision systems in the framework of hydrodynamics. This article begins with a brief review of that history, followed by an overview of observations from collisions of large nuclei such as gold and lead (Au+Au and Pb+Pb), supporting the standard hydrodynamic model of heavy ion reactions. Next we highlight the most important observations in small collision systems that provide evidence for similar underlying physics. We discuss key additional considerations and alternative explanations. Finally we review the current status of the theoretical interpretation of these results.

Before proceeding, a word on nomenclature is in order. In this review, we use “collective” as a generic descriptor for correlated particle production. If  $P(\vec{p}_1)$  is the probability to produce a particle with momentum  $\vec{p}_1$  in a collision, there is collective behavior if  $P(\vec{p}_1, \vec{p}_2) \neq P(\vec{p}_1)P(\vec{p}_2)$ . The nature of this correlation may be strictly at the two-particle level (e.g., resonance decay), or may extend to a broad number of particles, as in the case of jet production and (potentially) quantum interference effects. Hydrodynamic motion of a composite medium satisfies this definition of collective behavior, both at the two-particle and many-particle level. We emphasize that these terms apply to observations, while the real physics questions lie in understanding the causes; hadronization in the case of jet production, inter-particle interactions and/or fields in the case of hydrodynamics.

## 2. HISTORICAL PRELUDES

Collective models of nuclear matter have a long history that is replete with controversy and in some cases rancor. Certainly Bohr’s (2) compound nucleus and the associated liquid-drop model (building on work by Gamow, Heisenberg, and von Weizsäcker) (3) evoked little controversy, particularly after its quantitative success in explaining fission in  ${}^{235}\text{U}$  (4). The underlying physical assumption of quasi-equilibration of energy was plausible when applied to reactions involving slow neutrons. Collective descriptions of higher-energy collisions appeared to be less well grounded. Heisenberg’s (5) 1949 attempt to understand excitations of the pion fluid was widely ignored. By contrast, a year later Fermi’s (6) statistical model (which he acknowledged to be the extreme limit of Heisenberg’s approach) received considerable attention. Fermi argued that precisely because

---

<sup>1</sup>For an introduction to quark-gluon plasma properties, see the overview article that appears in this volume (1).

the interactions between pions and nucleons were strong, one could expect the available energy to be “rapidly . . . distributed among the various degrees of freedom according to statistical laws.” Taking the reaction volume as his only free parameter, Fermi developed predictions (in modern terminology) for particle multiplicities in terms of  $n$ -body phase space, and presented a simple argument showing that in the high-energy limit the number of produced particles  $N$  would vary with center-of-mass collision energy  $\sqrt{s}$  as  $N \sim s^{1/4}$ .

Fermi carefully qualified his statistical model’s extreme assumptions, noting that by working in the opposite regime from a perturbative approach, one might be able to bracket the correct theory. As noted by Anderson in Fermi’s *Collected Papers* (7), “In the later literature this made it appear that this theory was always wrong; a point that Fermi didn’t enjoy at all.” A special case of such criticism was voiced by Landau (8), who, after noting Fermi’s “ingenious idea,” writes that “the quantitative calculation given by him appears unconvincing to us and incorrect at several points.” In particular, Landau observes that the number of particles in the strongly interacting initial state is ill-defined [a point he attributes to Pomeranchuk (9)], and that the distribution of final-state particles may be calculated only at the endpoint of a hydrodynamic Landau (8) also stated that the hydrodynamic motion would be that of “an ideal (non-viscous and non-heat-conducting) liquid.” In subsequent research, Landau & Belenkij (10) elaborated on this assertion, noting that the condition for the applicability of hydrodynamics  $R \gg \ell_{\text{mfp}}$ , where  $R$  is the least dimension of the system and  $\ell_{\text{mfp}}$  is the mean free path, for a relativistic system necessarily leads to a large Reynolds number characteristic of inviscid systems. Expressing the Reynolds number in terms of the mass density  $\rho$ , the shear viscosity  $\eta$ , the bulk velocity  $V$  of the system, and the microscopic velocity  $v$  of its constituents, one has

$$\text{Re} \equiv \frac{\rho R V}{\eta} \sim \frac{\rho R V}{\rho \ell_{\text{mfp}} v} \sim \frac{R c}{\ell_{\text{mfp}} c} = \frac{R}{\ell_{\text{mfp}}} \gg 1 \quad . \quad (1)$$

Therefore, intrinsically relativistic systems in the hydrodynamic limit should have low (kinematic) viscosities.

Despite the pedigree of these early developments, it is fair to say that the hydrodynamic approach never entered the mainstream of hadronic physics in the second half of the twentieth century. Rather, a variety of methods—phase-shift analyses, S-matrix, bootstrap, and so forth—were investigated before QCD emerged as the underlying field theory for the strong interaction in the 1970s. Not even the excellent hydrodynamic description of inclusive hadron rapidity distributions at Fermi National Accelerator Laboratory (FNAL) fixed target energies and the CERN Intersecting Storage Ring (ISR) (11) was able to gain traction against the subsequent enthusiasm for QCD’s clear predictions for perturbative phenomena. One of the few exceptions to this general trend was Bjorken’s (12) simple and hugely influential model of hydrodynamic expansion in ultrarelativistic  $A + A$  collisions, which explicitly allowed for its application to  $p + p$  collisions.

Motivated by Bjorken’s predictions, there were experimental searches for signatures of QGP formation in  $p + p$  and  $\bar{p} + p$  collisions, including Tevatron experiments E735 (13) and Mini-MAX (14). No firm conclusions resulted from this program, in part due to the non-comprehensive

---

**Reynolds number:**

The dimensionless ratio of inertial forces to dissipative forces in a fluid.

**Shear viscosity:**

The larger the shear viscosity the more easily momentum can be exchanged between distant fluid cells and, consequently, the faster a gradient in fluid velocity (or a sound wave) dissipates into heat.

---

nature of these experiments; for example, MiniMAX exclusively searched for disoriented chiral condensates (DCC). In hindsight, the DCC searches serve as an important reminder that when a region of disturbed vacuum eventually returns to the normal vacuum via particle emission the final number of hadrons may not be the relevant quantity to understand whether collectivity or hydrodynamics is applicable at earlier times. In the case of E735, baryon and strangeness modifications in high-multiplicity events were a possible QGP signature, but the experiment also found explanations via autocorrelations between higher multiplicities and larger numbers of gluon jets. Recent measurements of strangeness enhancement of multi-strange baryons in  $p + p$  collisions at the LHC have revived this important discussion (15). The field pushed forward to study the collisions of the largest nuclei at relativistic energies, first in the fixed target programs at the Brookhaven Alternating Gradient Synchrotron (AGS) and CERN Super Proton Synchrotron (SPS), and ultimately with the construction of RHIC and the LHC.

### 3. STANDARD MODEL OF HEAVY ION COLLISIONS

In 2001, early results from the RHIC program indicated that in head-on Au+Au collisions at 200 GeV per nucleon pair, the majority of the energy is deposited into a medium whose expansion is well described hydrodynamically, that is, as a flowing fluid (16–19). The hydrodynamic nature of the matter was eventually quantified in terms of its shear viscosity, which turns out to be very close to the conjectured smallest possible ratio of viscosity to entropy density [ $\eta/s \geq \hbar/(4\pi k_B) = 1/4\pi$  in natural units] of any fluid (20, 21). This nuclear matter has a starting temperature of order 350–400 MeV, or equivalently four trillion Kelvin, and as such is composed of quarks and gluons no longer bound into color-neutral hadrons such as protons and neutrons. Subsequent measurements of Pb+Pb collisions at the LHC (22) at up to 5.02 TeV per nucleon pair display a similar fluidity with the matter starting at a higher initial temperature of order 400–600 MeV (23). In both cases, Au+Au and Pb+Pb collisions create a QGP that behaves as a nearly perfect fluid, that is, a fluid with  $\eta/s \sim 1/4\pi$ .

Just as the Big Bang theory is the prevailing paradigm for the time evolution of the early Universe, over the last 10 years the nuclear physics community has developed a Little Bang theory as the standard model for the time evolution of heavy ion collisions (described in detail in References 24–28). The evolution can be broken into distinct epochs:

- 1 The highly Lorentz-contracted nuclei collide with a very short traversal time ( $\ll 1 \text{ fm}/c$ ). Predominantly through interactions of gluons in the nuclei, often described in terms of gluon fields, energy is deposited into the newly created medium. The initial, very inhomogeneous, distribution of deposited energy in the transverse plane, perpendicular to the beam direction, is referred to as the initial condition.
- 2 The matter is initially out of equilibrium, and some time is required for it to equilibrate. During this time the matter expands at nearly the speed of light in the longitudinal direction and begins to expand radially in the transverse plane. This is often referred to as the pre-equilibrium stage.

---

**Lattice QCD:**

Numerical solution of QCD using a space-time lattice.

**Polyakov loop:**

A gauge-invariant quantity which is zero in the confining phase and non-zero in the deconfined phase of QCD.

**Bulk viscosity:**

A measure of the internal resistance of a fluid to expansion or compression.

---

- 3 After the matter is nearly equilibrated,<sup>2</sup> it is modeled via viscous hydrodynamics using an equation of state from lattice QCD calculations. Deviations from equilibrium are accounted for with shear and bulk viscosity terms.
- 4 The fluid cools to a temperature corresponding to the QGP crossover transition (32)  $T \approx 170$  MeV (as determined by the inflection point of the Polyakov loop, roughly equivalent to the confinement–deconfinement transition) (33) and then breaks up into hadrons, as most commonly modeled via Cooper–Frye freeze-out (34).
- 5 The resulting hadrons scatter, both inelastically, until what is called chemical freeze-out, and elastically, until kinetic freeze-out, at which time they are assigned their final-state momenta as measured experimentally.

Sophisticated computer modeling of large numbers of individual collisions follow each of these stages through to predictions for final hadrons that are measured experimentally. As with constraining properties of the early Universe, this field has advanced to multiparameter Bayesian analyses (35–39) to extract key properties of the medium, such as  $\eta/s$ , and to assess the correlated sensitivities of the extracted values to different assumptions for the initial conditions.

The matter produced in the collision is subjected to enormous longitudinal pressure, expanding at nearly the speed of light in this direction, often assumed to be boost invariant (12). There are also large pressure gradients in the transverse direction driven not only by the density differential to the vacuum outside the medium but also by inhomogeneities in the matter. Figure 1a shows the temperature and flow profile of an  $A + A$  collision from a hydrodynamic model. A number of key features are worth describing in detail:

1. There is an overall pattern of strong radial outward expansion with the largest bulk velocities near the periphery reaching 75% of the speed of light.
2. At the end of the hydrodynamic epoch, one calculates the hadronization process in the rest frame of the fluid cell and then boosts hadrons into the lab frame. Thus, heavier hadrons receive a larger momentum shift (blue-shift) that is measurable as a distinct feature in the transverse momentum ( $p_T$ ) distribution of hadrons as a function of their mass.
3. The spatial distribution of the matter and its temperature profile are lumpy, despite the lumpiness of the initial condition already having been washed out to some degree by viscous effects. These inhomogeneities lead to substantial distortions in the azimuthal distribution

---

<sup>2</sup>For most of a decade, since the identification of the applicability of hydrodynamics to heavy ion collisions, the predominant thinking has been that for hydrodynamic calculations to be valid the system must be nearly equilibrated at an early time of order  $\tau \approx 0.5\text{--}2.0$  fm/ $c$ . Thus the time before this point is referred to as pre-equilibrium, and an entire sub-area of the field has been devoted to the rapid equilibration puzzle, trying to answer the question of how the system equilibrates so fast. However, it was recently realized that the hot nuclear matter may never come close to equilibration (29–31) and that a different explanation justifies the applicability of hydrodynamics, as we discuss in detail in Section 6. In this picture, the separation of stages 2 and 3 is really only hydrodynamization (the point where hydrodynamics is applicable), and the naming of stage 2 as pre-equilibrium is misleading and should be simply pre-hydrodynamization.

of particles (40), which are quantified in terms of a Fourier expansion (41) as

$$\frac{dn}{d\phi} \propto 1 + \sum_n 2v_n(p_T) \cos[n(\phi - \Psi_n)] \quad , \quad (2)$$

where  $p_T$  and  $\phi$  are the transverse momentum and azimuthal angle of each particle and  $\Psi_n$  is the overall orientation of the  $n$ th moment. The first four moments,  $v_1$ ,  $v_2$ ,  $v_3$ , and  $v_4$ , are often referred to as directed, elliptic, triangular, and quadrangular flow coefficients, respectively.

4. Near mid-rapidity, for semi-central collisions, the dominant Fourier coefficient is  $v_2$ , reflecting the efficient hydrodynamic translation via pressure gradients of the initial almond-shaped overlap region to momentum space. Again, because of the larger fluid velocities built up along directions of steeper pressure gradients, heavier hadrons will have their flow patterns  $v_n(p_T)$  shifted outward in  $p_T$  (Figure 1b).

Hydrodynamic calculations describe the measured higher-order coefficients  $v_3$  to  $v_5$  (42). Such comparisons constrain both the initial inhomogeneities that are the source of the fluid anisotropies and the medium properties such as the shear viscosity, which has a larger damping effect on the higher-order coefficients. There is a nice analogy between these  $v_n$  measurements in heavy ion physics reflecting the initial spatial anisotropies and the spherical harmonic moment measurements from the cosmic microwave background reflecting the earlier inhomogeneities in the early Universe, providing key constraints on QGP properties from the former and early Universe properties from the latter.

The standard model of  $A + A$  collisions has now been well established and tested with great precision. This model describes a multitude of experimental measurements including the mass-dependent  $p_T$  spectra, the  $v_n$  flow coefficients, the distribution of event-by-event fluctuations in those flow coefficients, multiparticle correlations referred to as cumulants (44), and Hanbury Brown Twiss (HBT) correlations (45). Other correlations between different flow coefficients that only arise from the nonlinear mode mixing terms in hydrodynamics (46) are qualitatively described, leading Heinz & Snellings (25) to refer to this as an *experimentum crucis* in support of the hydrodynamic paradigm. There are some outstanding puzzles that may turn out to be reconciled within the standard framework [as was the case for the so-called HBT puzzle (47)], or be the first hints of additional physics. Specific examples include the flow moment ordering in ultra-central collisions (48) and thermal photon emission and anisotropy (49).

## 4. SMALL SYSTEM EXPERIMENTAL DATA

In the early years of the heavy ion collider era, small colliding systems such as  $p(d, {}^3\text{He})+A$  were regarded as control measurements. Measurements in  $d+\text{Au}$  and  $p+\text{Pb}$  collisions at RHIC and the LHC have been very useful, for example, in constraining nuclear modified parton distribution functions (nPDFs) that determine the initial gluon distributions that determine the first epoch of heavy ion collisions (50, 51). However, in 2010, the CMS Collaboration examined ultrahigh-

---

**Transverse momentum  $p_T$ :** The component of a particle's momentum  $p$  that is transverse to the collision axis,  $p_T \equiv p \cos \theta$ , where  $\theta$  is the particle's polar angle with respect to the collision axis.

**Central and off-central:** Ions colliding head-on are called central collisions, whereas if the ions only partially overlap the collision is semi-central or peripheral.

---

**HBT correlations:** Correlations at low relative momentum between two identical particles that are sensitive to the size and shape of the emission region, named after Hanbury Brown (one person) and Twiss, who developed this method in astronomy.

**Momentum rapidity  $y$ :**  $\cosh(y) \equiv \gamma$ , with  $\gamma = 1/\sqrt{1 - v_z^2}$ , with  $v_z$  the velocity along the beam direction in units of the speed of light.

**Pseudorapidity  $\eta$ :** A mapping of the polar angle  $\theta$  (with respect to the collision axis) of a particle, defined as  $\eta = \frac{1}{2} \log \frac{1 + \cos \theta}{1 - \cos \theta}$ . For massless particles pseudorapidity  $\eta$  and momentum rapidity  $y$  are identical; for highly relativistic particles rapidity and pseudorapidity are nearly equivalent.

---

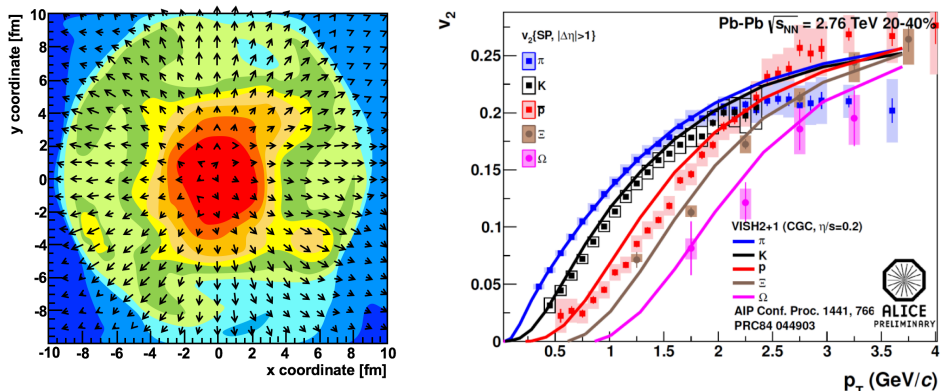


**Figure 1**

(a) Viscous hydrodynamic calculation results of a semi-central  $A + A$  collision in one time snapshot ( $t = 5$  fm/c). The color scale indicates the temperature of the fluid cells in the transverse ( $x$ - $y$ ) plane, and the arrows represent the fluid velocity vectors with the lengths proportional to the speed. (b) Elliptic flow coefficient  $v_2(p_T)$  for identified hadrons in Pb+Pb collisions at the LHC, also compared with hydrodynamic calculations (43).

multiplicity  $p + p$  collisions at the LHC and found that particles had a weak, though clear, preference to be emitted along a common transverse  $\phi$  angle across all rapidities (52). This finding sparked a scientific debate over whether this could be related to similar correlations observed in  $A + A$  collisions, or was due to new physics coming from momentum correlations present in the earliest moments of the collision. Then in 2012,  $p$ +Pb data taking at the LHC, quickly followed by a reexamination of  $d$ +Au data at RHIC, revealed that most of the signatures for hydrodynamic flow in  $A + A$  collisions also existed in these smaller systems. The revolution started by these small system measurements, and the attempt to reconcile them in the context of the heavy ion standard model, is the focus of this review. We concentrate on those observables most directly related to collectivity while noting that there is a wealth of data not included on electroweak probes, strangeness enhancement, and so forth, and additional physics areas of interest regarding nPDFs, gluon saturation phenomena, multiparton interactions, and color reconnection, among others.

#### 4.1. Two-Particle Correlations and Initial Observations

Crucial information regarding collectivity is garnered through the measurement of two or more particle correlations, often parameterized via the particles' relative azimuthal angle  $\Delta\phi$  in the



transverse plane, and their relative longitudinal pseudorapidity  $\Delta\eta$ . Since the reaction plane angles  $\Psi_n$  in Equation 2 are assumed to reflect geometric features of the initial matter distribution common to all produced particles, standard Fourier properties lead to two-particle correlations proportional to  $v_n^2 \cos(n\Delta\phi)$  that extend long-range in pseudorapidity as the matter expands longitudinally. Figure 2 shows two-particle correlations as a function of relative angles  $\Delta\phi$  and  $\Delta\eta$  as measured in  $p+p$ ,  $p+\text{Pb}$ , and  $\text{Pb}+\text{Pb}$  collisions at the LHC. In the  $\text{Pb}+\text{Pb}$  case, the long-range correlations dominate and were originally referred to as the ridge around  $\Delta\phi = 0$  and another ridge around  $\Delta\phi = \pi$ . In central collisions this second feature split into two ridges near  $\Delta\phi \approx 2\pi/3$  and  $4\pi/3$  and for a time were mistakenly interpreted as a Mach cone response from high-energy quarks traversing the matter. These features are now understood in a fully unified picture (53) as arising from elliptic, triangular, and higher flow moments.

However, there are a number of sources for such correlations having nothing to do with a flowing medium. In a hydrodynamic description, all of these other correlation sources are referred to as non-flow. Simple examples include the decay of hadronic resonances, such as  $\Delta^{++} \rightarrow p+\pi^+$ , giving rise to a two-particle correlation. Large momentum-transfer scattering of partons from the incoming hadrons or nuclei can result in jets, that is, two collimated sprays of hadrons that are nearly back to back in azimuth ( $\Delta\phi \approx \pi$ ) and with a correlation in pseudorapidity depending on the momentum fractions  $x_1$  and  $x_2$  of the incoming partons. Even low momentum-transfer scattering of initial partons can result in long-range correlations in pseudorapidity as a consequence of total momentum conservation. These contributions are evident in correlation measurements in all collision systems from  $e^+e^-$ ,  $p+p$ , and  $A+A$  to varying degrees and must be accounted for in order to isolate the contribution from flow physics.

In the  $\text{Pb}+\text{Pb}$  case, in addition to the dominant flow contributions, there is a localized peak near  $\Delta\phi \approx \Delta\eta \approx 0$  due to correlations among a small number of particles from single jet fragmentation, resonance decay, and so forth. Because hadrons from a single fragmenting jet are in a cone, they are easily distinguished from the long-range flow contribution around  $\Delta\phi = 0$ . However, the dijet partner, while approximately back to back in azimuth, can swing in pseudorapidity, resulting in a long-range correlation around  $\Delta\phi = \pi$ , which is more challenging to disentangle from flow. In the  $A+A$  case, these dijet correlations are subdominant for  $p_T < 5 \text{ GeV}/c$ . Figure 2 shows the same two-particle correlations in  $p+\text{Pb}$  and  $p+p$  collisions at the LHC. One observes the near-side ridge in both cases, although with weaker strength, and a larger away-side ridge, from the combination of flow correlations and non-flow contributions. These features represent the first evidence of flow-like collective behavior in a small system: High-multiplicity  $p+p$  collisions at the LHC exhibit a long-range near-side ridge in azimuthal correlations, very similar to that observed in  $A+A$  collisions. Because of the unexpected nature of the ridge as a flow signature in small systems (though not unexpected by all; e.g., (54)) and the inability to determine whether there was a contribution on the away side underneath the dijet signal, there was speculation of possible new physics at play having nothing to do with the initial geometry followed by collective expansion. We discuss these alternative scenarios in Section 5.4.

In 2012,  $p+\text{Pb}$  collisions at  $\sqrt{s_{NN}} = 5.02 \text{ TeV}$  were first run at the LHC, and immediately all of the collaborations published similar flow observations [see, e.g., results from ALICE (56),

---

**Near and away side:**

Near-side refers to the region in azimuthal angle  $\phi$  near a high transverse momentum particle or jet “trigger”. Away-side is the region at relative azimuthal angle (with respect to the near-side trigger)  $\Delta\phi \approx \pi$ .

---

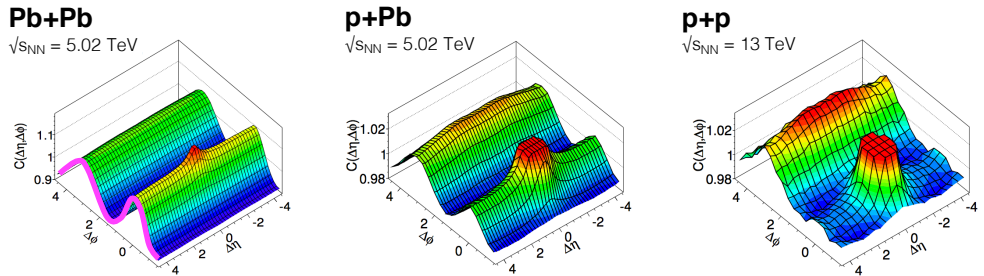


**Figure 2**

Two-particle correlation results in (a) Pb+Pb, (b)  $p$ +Pb, and (c)  $p$ + $p$  collisions at the LHC (55). In Pb+Pb collisions there is a large  $\cos(2\Delta\phi)$  correlation with peaks at  $\Delta\phi = 0, \pi$  that extend long-range in pseudorapidity  $\Delta\eta$  (magenta curve). A similar feature is observed in  $p$ +Pb and  $p$ + $p$  collisions, though it does not dominate the overall correlations to the same degree.

**Jet quenching:** The suppression of high transverse momentum particle and/or jet production relative to yields expected from the number of hard scatters in a collision.

ATLAS (57), and CMS (58)]. Here the experimental signatures were much stronger than in  $p$ + $p$  collisions, and the race was on to repeat as many of the  $A$ + $A$  measurements related to collectivity as possible to determine whether the signals persisted in  $p$ +Pb. Experimenters at RHIC immediately reexamined  $d$ +Au collision data at  $\sqrt{s_{NN}} = 200$  GeV from 2008 and found similar patterns, though with a smaller flow signal relative to the non-flow backgrounds (59). To date, nearly all observations in  $A$ + $A$  collisions that provided strong evidence for the heavy ion standard model “quark–gluon plasma as near-perfect fluid” have now been measured in  $p$ +Pb and  $d$ +Au collisions (see Reference (60) for an excellent review). The notable exception to this statement is jet quenching, which is discussed in Section 5.1.

## 4.2. Instructive Measurements

In this section we discuss four particularly instructive measurements in small systems, each of which tests a key aspect of extending the heavy ion standard model to such systems. These measurements involve (a) multiparticle cumulants demonstrating that correlations exist among the majority of emitted particles as opposed to a small subset, (b) manipulation of the colliding small nuclei to see whether the correlations scale as expected with initial geometry, (c) particle-identified flow patterns to see whether they reflect a common velocity field of a fluid at hadronization, and (d) higher moments of the flow patterns, including triangular and quadrangular flow.

**4.2.1. Multiparticle cumulants.** In a collision creating  $N$  particles, one can ask whether a given two-particle correlation is indicative of correlations involving only a small subset of particles  $M \ll N$  (as in the dijet case), or from  $M \approx N$ , that is, a feature of the bulk. Most non-

hydrodynamic explanations for the observations in small systems invoking finite-size momentum domains predicted the former case, whereas an overall flowing medium implies the latter case. Multiparticle cumulants utilize sets of 2, 4, 6, ...,  $n$  particles that sequentially subtract away correlations among only  $n - 2$  particles, with an extension to all  $N$  particles using the Lee–Yang zeros method (61, 62). These measurements have been particularly powerful because in the small-variance Gaussian limit the two-particle and four-particle results can be written as  $v_2\{2\} = \sqrt{\bar{v}_2^2 + \sigma^2}$  and  $v_2\{4\} \approx \sqrt{\bar{v}_2^2 - \sigma^2}$ . They therefore allow extraction of both the event-averaged  $\bar{v}_2$  and the event-by-event variance  $\sigma^2$  (63). This has established in  $A + A$  collisions at RHIC and the LHC a direct quantitative connection between the event-by-event variation in the initial geometry and the flow fluctuations(64).

Figure 3 shows  $v_2$  multiparticle cumulants as measured in  $p + p$ ,  $p+\text{Pb}$ , and  $\text{Pb}+\text{Pb}$  collisions at the LHC (65–69). The splitting of  $v_2\{2\} > v_2\{4\}$ , as related to flow fluctuations, is also observed in  $p+\text{Pb}$  collisions, yet disappears in the  $p + p$  case. In 2016, RHIC had a special run of  $d+\text{Au}$  collisions over a range of energies (200, 62.4, 39, and 19.6 GeV) to address how low in energy these features persist. The results from the  $d+\text{Au}$  collisions at 200 GeV on the two-, four-, and six-particle cumulants also indicate that the correlations are at the multiparticle level (70).

We note that nonzero multiparticle cumulants are not unique to a hydrodynamic description (e.g., 60, 71). Imagine a flock of birds in flight that have  $N$ -body correlations, where

order can be the effect of a top-down centralized control mechanism (for example, due to the presence of one or more leaders), or it can be a bottom-up self-organized feature emerging from local behavioral rules. The prominent difference between the centralized and the self-organized paradigm is not order, but response (72).

Thus, the key connection is the relation of cumulants to the response to initial geometry, rather than the mere real-valued <sup>3</sup>  $v_2, v_4, v_6$ , and so forth.

In summary, the multiparticle measurements in  $A + A$ ,  $p+\text{Pb}$ , and  $d+\text{Au}$  collisions at RHIC and the LHC yield strong evidence for  $N$ -body correlations, providing a connection to the fluctuating initial conditions. However, in the lower-multiplicity cases of  $p + p$  at the LHC and  $p+\text{Au}$  and lower-energy  $d+\text{Au}$  at RHIC, the cumulants do not follow the expected small variance expectation, which may not be surprising as the fluctuations and non-flow effects are larger. More research will be needed (e.g., (73)) to resolve these questions.

**4.2.2. Manipulating the geometry.** The initial small system flow measurements at RHIC were made in  $d+\text{Au}$  (59) rather than  $p+\text{Au}$  collisions, due to accelerator constraints. However, it was noted that in a  $d+\text{Au}$  central collision, the projectile neutron and proton from the deuteron deposit energy in two hot spots, thus yielding a very different initial condition than the single hot spot in a  $p+\text{Au}$  collision (74). This key observation (75) led to a systematic program of

---

<sup>3</sup>The  $v_n$ 's extracted using cumulants can assume complex values when large fluctuations and/or non-flow effects dominate the flow signal.

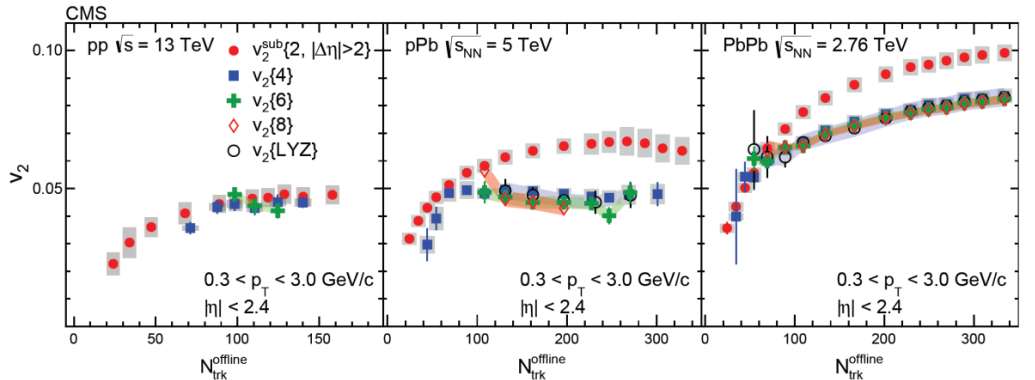


**Figure 3**

The  $v_2$  multiparticle cumulants as a function of charged-particle multiplicity for (a)  $p + p$ , (b)  $p + \text{Pb}$ , and (c)  $\text{Pb} + \text{Pb}$  collisions at the LHC (69).

injecting different initial-state asymmetries through  $p$ ,  $d$ , and  ${}^3\text{He}$  projectiles incident on Au nuclei at RHIC (76–78). Figure 4a shows that the various projectiles result in initial conditions that are dominantly circular, elliptical, and triangular for  $p$ ,  $d$ , and  ${}^3\text{He}$  projectiles, respectively. Figure 4b shows theoretical predictions from the hydrodynamic standard model (75) that are in excellent agreement with the subsequent experimental measurements of  $v_2$ . In addition, the  ${}^3\text{He}$  projectile was chosen to enhance triangular initial geometries, and the triangular flow  $v_3$  has also been measured and is in agreement with theoretical predictions (77).

The agreement with data requires a full modeling of both the initial conditions and the subsequent evolution. In the case of  $d + \text{Au}$  and  ${}^3\text{He} + \text{Au}$ , the initial geometry is dominated by the location of the two or three nucleons at the point of impact. In contrast, for  $p + \text{Au}$ ,  $p + \text{Pb}$ , and in particular  $p + p$  collisions, the initial geometry depends critically on the modeling of sub-nucleonic degrees of freedom (discussed in Section 5.2). The simultaneous description of the three engineered geometries at RHIC yields compelling evidence that the dominant correlation source can be related to initial geometry coupled with subsequent interactions or fluid dynamics. As of early 2018, no alternative explanation has been successfully put forward to describe these observations.

**4.2.3. Mass-ordering fingerprint.** As noted in the  $A + A$  case, there is a distinct ordering of  $v_2$  as a function of  $p_T$  for different hadron species. This ordering is often referred to as the fingerprint of a flowing fluid because it is the velocity of each fluid element as it hadronizes that results in different momentum boosts for the hadrons of different mass. Figure 5 shows the mass dependence of  $v_2$  in  $p + p$  (69),  $d + \text{Au}$  (76), and  $p + \text{Pb}$  (79) collisions, along with viscous hydrodynamic model comparisons in the last two cases. The agreement between data and theory in the  $d + \text{Au}$  and

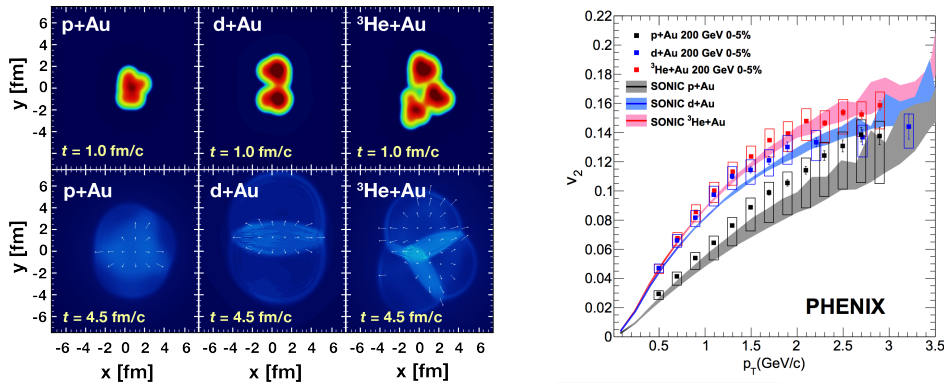


**Figure 4**

(a) Calculations of (*top*) the initial energy density in  $p+\text{Au}$ ,  $d+\text{Au}$ , and  $^3\text{He}+\text{Au}$  collisions at RHIC and (*bottom*) the resulting hydrodynamic evolution utilizing Monte Carlo Glauber initial conditions (75). (b) Comparison between hydrodynamic calculations (75) and data from  $p+\text{Au}$ ,  $d+\text{Au}$ , and  $^3\text{He}+\text{Au}$  collisions at  $\sqrt{s_{NN}} = 200$  GeV (78).

$p+\text{Pb}$  cases at RHIC and LHC energies is another check on the heavy ion standard model.

**4.2.4. Initial-state fluctuations and higher moments.** A big step forward in solidifying the standard model for  $A+A$  collisions was the incorporation of nucleon-level fluctuations for understanding the initial conditions and the resulting higher-order flow coefficients. For the  $p+p$  and  $p+\text{Pb}$  cases, sub-nucleon-level fluctuations are crucial, as discussed below in Section 5.2. Figure 6 shows the measured  $v_2$ ,  $v_3$ , and  $v_4$  coefficients as a function of  $p_T$  in  $p+p$ ,  $p+\text{Pb}$ , and  $\text{Pb}+\text{Pb}$  central collisions at LHC energies (81). Also shown are calculations from the SONIC implementation of the heavy ion standard model starting with initial conditions based on sub-nucleonic structure and  $\eta/s = 1/4\pi$ . Within the unified framework of the heavy ion standard model, one achieves agreement for all three systems and for all orders of  $v_n$ .

### 4.3. Limits of Small System Flow Behavior

All of these results engender the question: How low in deposited energy, or in final particle multiplicity, does the experimental data exhibit correlations that match viscous hydrodynamic calculations? There are two different experimental ways to attack this question: (a) examining lower-multiplicity  $p+p$  interactions and (b) examining small system collisions at lower energy. After the initial discovery of the  $p+p$  ridge at the LHC in collisions at 0.9–7 TeV, follow-up

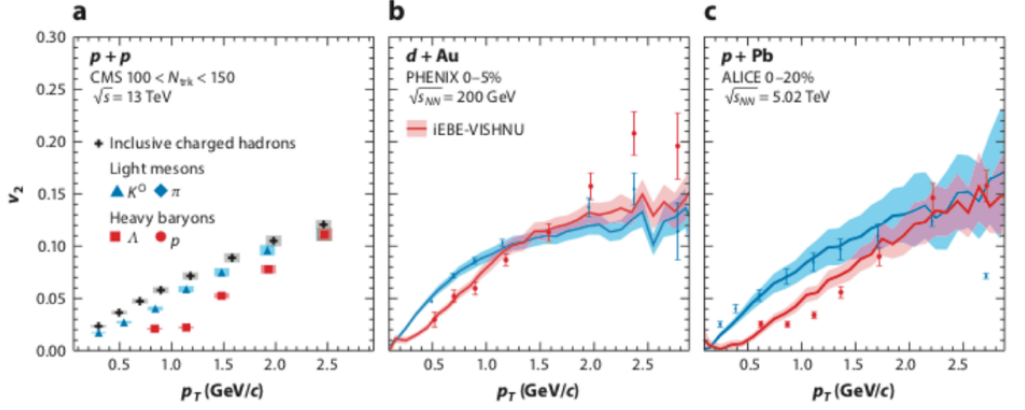


**Figure 5**

Elliptic flow coefficient  $v_2$  as a function of  $p_T$  for different hadron species as measured in different small systems: (a)  $p + p$  at the LHC, (b)  $d + \text{Au}$  at RHIC, and (c)  $p + \text{Pb}$  at the LHC. Theory calculations utilizing the hydrodynamic standard model are from Reference (80).

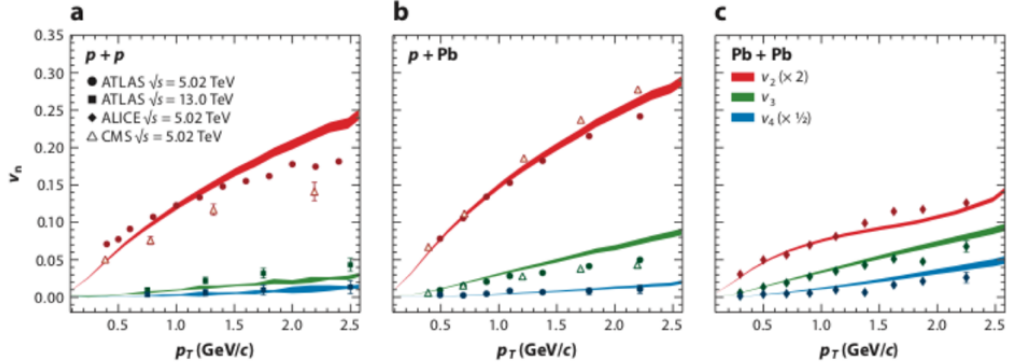


**Figure 6**

Experimental data for momentum anisotropies  $v_2$ ,  $v_3$ , and  $v_4$  as a function of  $p_T$  in (a)  $p + p$ , (b)  $p + \text{Pb}$ , and (c)  $\text{Pb} + \text{Pb}$  collisions at the LHC. Also shown are hydrodynamic standard model (superSONIC) calculations that incorporate constituent quark Monte Carlo Glauber initial conditions, pre-equilibrium dynamics, viscous hydrodynamics with  $\eta/s = 1/4\pi$ , and hadronic scattering (81).

measurements in  $p + p$  collisions at higher energies of up to 13.1 TeV revealed an even stronger signal. However, for  $p + p$  collisions of lower multiplicity, the non-flow contributions increase and a reliable extraction of the flow signal becomes model dependent. ATLAS (55) and CMS (69)

employ different extraction methods and currently come to different conclusions regarding when the flow signal disappears.

The other way to pursue this question is with the  $d$ +Au beam energy scan at RHIC. In this case, one has better control over the initial geometry while changing the energy deposition and the total particle multiplicity, albeit with larger theoretical uncertainties due to the unknown variation of the transport coefficients and the equation of state with the increasing baryon chemical potential. Calculations within the hydrodynamic framework predicted a rather modest decrease in the flow signal (82, 83). The PHENIX Collaboration (84) has reported results on  $v_2$  as a function of collision energy (200, 62.4, 39, and 19.6 GeV). Figure 7 shows the measured  $v_2$  coefficients as a function of pseudorapidity for high-multiplicity  $d$ +Au collisions at the three higher energies. The measured  $v_2$  shows little energy dependence, in reasonable agreement with hydrodynamic calculations. Also shown are parton transport model calculations that are described in detail in Section 5.3. In  $d$ +Au central collision data at 200 GeV, as noted above, there is additional evidence from the two-, four-, and six-particle cumulants that the anisotropy is a bulk  $N$ -particle correlation dominated by the translation of initial geometry into momentum space. The flow signal via cumulants appears to persist down to the lowest energies measured, though masked by a growing non-flow contribution to the correlations. The question of how small or low in energy these collective features persist remains outstanding, and its resolution may hinge on whether one can perfectly factorize the flow and non-flow contributions.

---

**Transport coefficients:** parameterize the relaxation rate of a system in response to a gradient taking it out of equilibrium. Examples include the thermal conductivity, electrical conductivity, and shear and bulk viscosities.

---

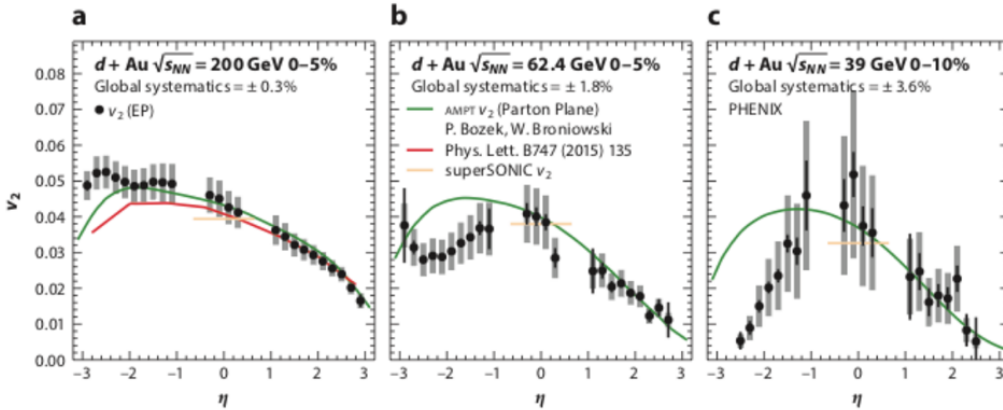


**Figure 7**

Measured  $v_2$  integrated over  $p_T$  as a function of pseudorapidity from  $d$ +Au collisions at (a) 200, (b) 62.4, and (c) 39 GeV. Also shown are calculations within the standard hydrodynamic framework (red and orange curves), as well as calculations from the parton and hadron transport framework AMPT (A Multi-Phase Transport Model).

---

**quasiparticles:**

quasiparticles are excitations in a system with lifetimes long compared to the mean time between collisions, thereby allowing for a particle-like description of their transport properties.

---

## 5. ADDITIONAL CONSIDERATIONS

Several additional considerations are important to include in any discussion of small system heavy ion physics. Here we discuss two key topics that must be reconciled when applying the heavy ion standard model to these small systems: (a) the apparent absence of jet quenching effects in small collision systems and (b) the influence of modeling the initial conditions at the sub-nucleonic level. In addition, there are proposed alternative interpretations of the small system data that include (a) parton scattering models with well-defined quasiparticles and (b) initial-state momentum correlation models. We discuss these considerations in detail in the next four subsections.

### 5.1. Jet Quenching in Small Collision Systems?

In  $A + A$  collisions, an important confirmation of the heavy ion standard model comes from the energy loss of high- $p_T$  partons traversing the medium, referred to as jet quenching (85–87). Jet quenching models calculate the rate and kinematics for hard scattering, that is, large momentum-transfer interactions, and then propagate the resulting partons through the space-time evolution of the matter calculated from hydrodynamic codes. Jet quenching was discovered at RHIC in Au+Au collisions as a factor-of-five suppression of high- $p_T$  hadrons relative to their expected rate from scaling up  $p + p$  yields (88). A critical observation made in 2003 was that this quenching effect disappeared in  $d+Au$  collisions where no dense medium was expected 89–92. No suppression was observed in  $d+Au$  collisions; thus, at the time, jet quenching was confirmed as an exclusively final-state effect from the medium in  $A + A$  collisions. Similar measurements at the LHC of single hadrons in Pb+Pb and  $p+Pb$  collisions (Figure 8a) (93) demonstrate the quenching observed in  $A + A$  collisions is not observed in small systems. Modern measurements including fully reconstructed jets and jet structure provide further evidence for quenching-related modifications in  $A + A$  but not in  $p + A$  collisions.

It now may seem surprising that no jet quenching effect is apparent in  $p + A$  collisions if indeed a hot medium is formed. How can there be a medium created that is described by hydrodynamics, and that significantly modifies the distribution of final-state hadrons, yet has no significant impact on the distribution of high- $p_T$  particles? The jet quenching effect in  $A + A$  collisions becomes more prominent in more central, higher-multiplicity reactions as the average in-medium path the partons traverse correspondingly grows. In small systems, the medium created is smaller, so the average path is expected to be significantly shorter. One possibility is that after the hard scattering the parton is in a highly virtual state, and its evolution may be only modestly affected by scattering with other partons in the medium. As such, a long medium traversal time, as in central  $A + A$  collisions, encompasses a parton where the medium scattering significantly modifies the parton shower, but in a  $p + A$  collision with short medium lifetimes ( $\tau < 2\text{--}4$  fm/ $c$ ) the jet quenching may be much smaller.

Quantitative theoretical calculations of the expected quenching effects in small systems have been made (e.g., 94–96), though no clear consensus on the magnitude of the quenching has been reached. The lack of quenching observed in Figure 8a is observed in minimum bias collisions—that is, averaged over all geometries. Many calculations predict observable quenching effects



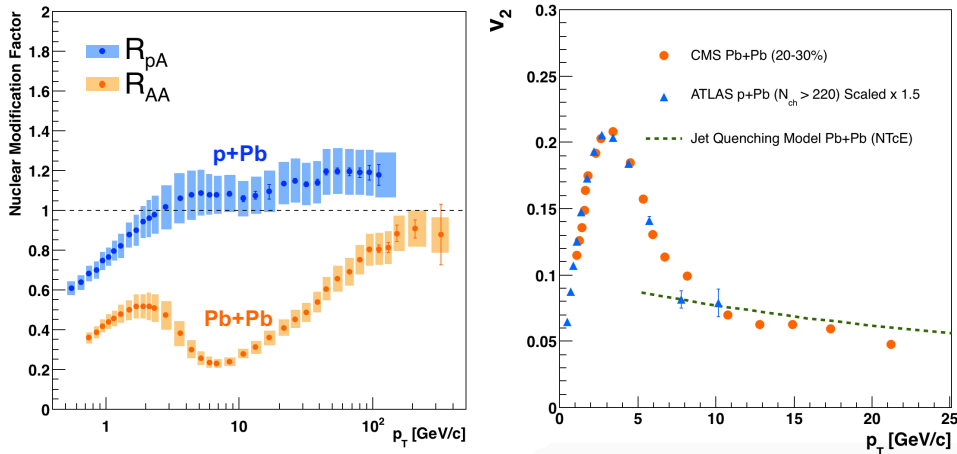


**Figure 8**

(a) The nuclear modification factor  $R_{AA}$  for unidentified hadrons as a function of  $p_T$  (93). This factor is the ratio of yields in  $A + A$  collisions relative to scaled up  $p + p$  yields. One observes significant modification, namely suppression, in Pb+Pb collisions and almost no modification in  $p+Pb$  collisions. (b) The  $v_2$  coefficient for hadrons as a function of  $p_T$  in Pb+Pb and  $p+Pb$  collisions at the LHC. The  $p+Pb$  results have been scaled up by a factor of 1.5 for shape comparison. The green dotted curve (94) is from a jet quenching calculation where the anisotropy results from the directional dependence of the energy loss, rather than hydrodynamic flow.

in central or high-multiplicity  $p+Pb$  collisions where the paths traversed by the partons may be longer. However, in these small systems, the selection of event classes based on multiplicity has strong autocorrelations between the nature of the nucleon–nucleon collisions and the hard process itself, which complicate the interpretation of experimental observables. When selecting on multiplicity classes, jets and high- $p_T$  hadrons are suppressed in central events (as expected from jet quenching), but are counterbalanced by an equal-magnitude enhancement in peripheral events—thus resulting in no modification when averaging over all  $p + A$  collisions (97). The suppression in central events is widely interpreted in terms of this autocorrelation bias, that is, pushing more events with jets into the most central category via multiplicity, rather than the result of jet quenching (98). Recent results with event class selected on spectator neutrons, and thus with reduced autocorrelation bias, indicate little or no quenching in more central event categories (99).

One mystery involves the measurement of  $v_2$  for hadrons at large  $p_T$ . In the  $A + A$  case, the azimuthal anisotropy  $v_2$  is interpreted in terms of flow for low- $p_T$  particles. In contrast, at high  $p_T$ , hadrons have a more modest anisotropy in  $A + A$  collisions (Figure 8). This anisotropy is thought to result from jet quenching, with partons losing more energy when traversing a longer path through the medium. What is striking is that the  $v_2$  measured in  $p+Pb$  (100) scaled by a

---

**Spectator:** Nucleon that does not collide and hence keeps on moving along the beam direction.

---

factor of 1.5 (Figure 8b) appears to follow the same pattern. If there is no jet quenching in  $p$ +Pb events, what else could be the source of the anisotropy at high  $p_T$ ?

Jet quenching is a fertile area of investigation and part of the motivation for comparing a full suite of jet measurements at RHIC from the new sPHENIX detector (101) to observations at the LHC over a range of collision system sizes. New measurements of charm and beauty hadrons in small systems are also expected to be illuminating. In  $A + A$  collisions, bulk medium hydrodynamics and rare jet quenching probes provide complementary information on the system created, and the presence of the former and the apparent absence of the latter in small systems represent a crucial area where more data and theoretical work are needed.

## 5.2. Initial Conditions

Extracting medium properties from hydrodynamic calculations requires a good quantitative constraint on the initial geometry. The simplest such geometry is calculated via the billiard ball interaction picture encapsulated in Monte Carlo Glauber calculations (102). Within this framework, individual nucleons are distributed within a nucleus following the relevant Woods–Saxon functional form and the inclusion of a hard-core repulsive potential. Nucleons in the projectile and target then interact as dictated by the nucleon–nucleon inelastic cross section. The resulting energy or entropy is distributed in the transverse plane according to a two-dimensional Gaussian with a width parameter typically chosen as  $\sigma = 0.4$  fm. Extensions to this picture incorporate nondeterministic interaction probabilities, fluctuating nucleon sizes, and negative binomial fluctuations in energy deposition (e.g., 103, 104).

In the case of  $A + A$  collisions, the (extended) nucleon-level Monte Carlo Glauber framework is, for the most part, sufficiently constrained to provide confidence in the overall heavy ion standard model space-time evolution and extraction of matter properties such as  $\eta/s$  with precision. This methodology was developed over many years and includes refinements such as the inclusion of deformation parameters, particularly for uranium, as well as detailed studies of nucleon–nucleon correlations. In the case of  $d$ +Au and  $^3\text{He}$ +Au, respectively, the Hulthen wave function for the deuteron is well understood and for  $^3\text{He}$  the full three-body wave function has been solved ab initio. These calculations have shown that detailed substructure of the nucleon influences results only in the most central  $A + A$  collisions, where fluctuations are the dominant source of azimuthal anisotropies. However, in  $p + p$  and proton-induced nuclear collisions, sub-nucleonic structure dominates and casts a shadow over the predictive power of the standard heavy ion modeling.

Several studies of the influence of sub-nucleonic structure modeling have been carried out, and we describe here two such studies (see also 105, 106). The first utilizes the IP-Glasma framework (107), where the initial energy deposition is computed in terms of overlapping gluon fields. In this calculation the geometry of deposited energy follows the overlap regions between interacting nucleons; therefore, in central  $p$ +Pb and  $p$ +Au collisions it results in a very circular medium. This circular initial condition coupled with hydrodynamic evolution underpredicts the  $v_2$  in  $p$ +Au and  $p$ +Pb by up to a factor of four (108). Thus, with very little initial eccentricity

---

**Glasma:** A hypothesized precursor state to quark-gluon plasma where the color fields of the gluons form a classical coherent field with amorphous structure similar to glasses.

---

the medium simply expands radially with no strongly preferred axis. A second method utilizing the proton form factor (109) also results in a very circular initial conditions and, in particular for  $p + p$  collisions, predicts a vanishing  $v_2$  for the highest-multiplicity collisions.

Another approach is to include the simplest extension of the sub-nucleonic picture by assuming the proton is decomposed into three valence quarks, each with a cloud of gluons around it, and that each valence quark cloud interacts when it comes within some fixed distance of another such cloud. In much of the literature this picture is referred to as the constituent quark model. The hydrodynamic calculation shown in Figure 6 provides a reasonable description of  $v_2$ ,  $v_3$ , and  $v_4$  in  $p + p$ ,  $p+\text{Pb}$ , and  $\text{Pb}+\text{Pb}$  collisions using this constituent-quark-based Monte Carlo Glauber model for the initial geometry. Further substructure, smaller than these clouds, is expected to have a small influence, as a number of studies indicate that finer-scale structures are very quickly washed out.

The earlier IP-Glasma calculations have also been extended under the ansatz that the proton has a substructure with three gluon hot spots and then constraining their distribution with one additional free parameter fixed to match HERA  $e+p$  data (110, 111). Applying this updated proton substructure as initial conditions in  $p+\text{Pb}$  collisions, good agreement is found with many flow observables including higher moments (112).

An intriguing new development involves inverting the problem: If one posits viscous hydrodynamics as the correct model for the time evolution, then one can try to determine the initial condition and learn something about the structure of the proton on timescales that are short compared with the nucleus crossing time (106, 112). At RHIC energies, this may be feasible because one can test the hydrodynamic evolution hypothesis with  $d+\text{Au}$  and  $^3\text{He}+\text{Au}$  data that are not as sensitive to the initial condition model. There have also been attempts to simultaneously constrain medium properties and initial condition substructure within a Bayesian framework (35–39). This is an exciting prospect and should be fully pursued for small system geometries at RHIC and the LHC.

### 5.3. Parton Transport Models

In the 1990s parton transport models were developed that treated quarks and gluons as well-defined quasiparticles that scatter with one another. Early implementations such as VINI (113), ZPC (114, 115), and MPC (116) predicted rather modest collective effects (i.e., flow) due to the expected small QCD ( $2 \rightarrow 2$ ) parton–parton scattering cross section. Had these calculations proved accurate, the produced medium could accurately be termed a weakly coupled QGP. Instead, the first experimental data from RHIC with  $\text{Au}+\text{Au}$  collisions at  $\sqrt{s_{NN}} = 130$  GeV, indicating large elliptic flow, immediately presented a major challenge for these frameworks. For example, within MPC, only by artificially increasing the expected perturbative QCD parton–parton inelastic cross section from 3 mb to 45 mb could one describe the data (117, 118). The conclusion at the time was that the medium is strongly coupled; in other words, the parton–parton interactions are highly non-perturbative, and there are no well-defined quasiparticles. Thus, the system is amenable only to calculations with strong fields or hydrodynamic descriptors.

---

$\sqrt{s_{NN}}$ : is the total collision energy per nucleon-nucleon pair in the center of mass frame.

---

However, a new class of parton transport models has been developed that provide a better qualitative description of experimental data. Two such examples are the BAMPS (Boltzmann Approach to Multi-Parton Scatterings) (119) and AMPT (A Multi-Phase Transport) (120) models. The BAMPS model considers only gluon quasiparticles subject to  $gg \rightarrow gg$  scattering with a strong coupling  $\alpha_s = 0.6$  as well as higher-order scatterings of  $gg \rightarrow ggg$  and  $ggg \rightarrow gg$ . In the limit of many scatterings, BAMPS produces hydrodynamic-like flow patterns, and within this framework, a small effective  $\eta/s$  value near the lowest bound is extracted (121).

The AMPT model (120) has nearly massless quark and antiquark quasiparticles that are produced via a so-called string-melting mechanism. The produced quarks are allowed to scatter, hadronize via coalescence, and then undergo hadronic inelastic and elastic scattering. The implementation of only quarks and antiquarks enables a consistent recombination into hadrons via coalescence in the latter stage. This generator, though with many tunable components and various seemingly unphysical assumptions (e.g., no gluons), has successfully matched a number of  $A + A$  observables and provided insights into the translation of initial geometry into final hadron momentum anisotropies (most famously in Reference (53)). It was generally assumed that this was due to many scatterings that effectively modeled fluid flow, that is, approaching the hydrodynamic limit as the mean free path approaches zero in the transport picture. However, recently it was shown that the number of scatterings is quite modest, and for small systems at RHIC and the LHC the majority of partons have no scatterings at all. This realization has led to an understanding of the anisotropies as due to a differential probability to scatter or not—a so-called parton escape or tomographic image scenario (122). This puzzle is highlighted by the agreement (often quantitative) between AMPT and small system flow signals in  $p$ +Pb (123) and  $p$ +Au,  $d$ +Au, and  $^3\text{He}$ +Au collisions (124). Figure 7 shows an example of this agreement with calculations of  $v_2$  as a function of pseudorapidity in  $d$ +Au collisions at different energies (84).

An important set of outstanding questions includes the following: (a) Are these parton quasiparticle scattering scenarios a dual picture to hydrodynamics even with very small scattering probability, and (b) if not, are there key distinguishing experimental observables that can discriminate between the two? The latter question has proven challenging to answer since many observables are sensitive to the initial geometry and fluctuations, yet rather insensitive to the mechanism of translation into momentum anisotropies. Thus, AMPT describes  $v_2$ ,  $v_3$ , and  $v_4$  and their fluctuations at the same level as hydrodynamics when utilizing the same initial conditions. Observables one would naïvely expect to be more sensitive, such as the mass-dependent  $v_2$  splitting, are in fact qualitatively reproduced in AMPT, yet result from completely different physics—in this case from the hadronic scattering stage (125). Another observable is the correlation between flow moments, for example,  $v_2$  and  $v_4$ , that arise in hydrodynamics from nonlinear terms that result in mode mixing. However, AMPT calculations achieve a similar level of agreement with these mode-mixing observables (126).

These models are seemingly self-contradictory. Both AMPT and BAMPS have a short initial formation time for the partons to interact as well-defined quasiparticles and a mean free path between scatterings shorter than the de Broglie wavelength  $\lambda_{\text{dBg}}$ . In fact, in AMPT the initial parton formation time is approximately  $0.2 \times \lambda_{\text{dBg}}$ . Is it right to then state that a weakly

interacting system of partons is an alternate picture to the strongly coupled hydrodynamics when setting  $\alpha_s = 0.6$  and assuming mean free paths less than the de Broglie wavelength ( $\lambda_{\text{mfp}} < \lambda_{\text{dBg}}$ )? It is interesting to note that a precursor to the  $\eta/s \geq 1/4\pi$  bound was indeed derived in kinetic theory under the assumption that a particle mean free path could not be smaller than the shortest distance resolvable via the uncertainty principle, corresponding to the reduced de Broglie wavelength  $\lambda_{\text{dBg}}/2\pi$  (127). That said, the quantitative description of a large collection of experimental data implies that there is some key physics captured or mimicked in this approach. The field requires a concentrated effort in developing additional parton scattering models that are publicly available (as is AMPT) that will simplify the physics assumptions to understand how to reconcile or discriminate this quasiparticle picture from the strongly coupled hydrodynamic one.

#### 5.4. Momentum Correlations Explanations

Both viscous hydrodynamics and parton transport calculations have a common feature: The initial geometry of the deposited energy in the transverse plane is translated into azimuthal momentum anisotropies via final-state interactions, between either fluid elements or quasiparticles. In contrast, when long-range ridge correlations were first reported in high-multiplicity  $p + p$  collisions at the LHC (52), explanations emerged in which the correlations were generated in the initial scattering, that is, on the timescale of the nuclear crossing, and required no later-stage interactions or coupling. A number of these initial momentum correlation calculations are discussed in detail in Reference (128).

One proposal utilizes glasma graphs that produce correlated particles from different color flux tubes extended in rapidity with transverse separations less than the color-correlation length,  $1/Q_s$ , where  $Q_s$  is the saturation scale (129, 130). This picture results in back-to-back particle correlations (i.e.,  $\Delta\phi \approx 0, \pi$ ) that extend long-range in pseudorapidity. With  $Q_s \approx 1\text{--}2$  GeV, the transverse length scale is 0.1–0.2 fm. Thus, the correlation should exist only among a subset of the particles, and the correlation should be predominantly back to back, resulting in a significant  $v_2$  but no significant  $v_3$  or higher moments. The measurement of multiparticle correlations and higher-order anisotropy coefficients in small systems at RHIC and the LHC present a challenge for these pictures. Recent research including additional diagrams indicate that these features may be recovered at a qualitative level (see Reference (131) for a summary).

A key test of the momentum domain pictures comes from the geometry tests with  $p+\text{Au}$ ,  $d+\text{Au}$ , and  $^3\text{He}+\text{Au}$  collisions at RHIC. The momentum correlations originate in a local domain size of order 0.2 fm, which is quite small compared with the deuteron root-mean-square diameter of 4.2 fm. Thus, a natural prediction of these locally generated correlations is that the signal should be smaller in  $d+\text{Au}$  collisions than in  $p+\text{Au}$  collisions. In the  $d+\text{Au}$  case, each domain is contained in only one local hot spot originating from either the proton or neutron from the deuteron, so the final correlation is diluted by the particles emitted from the other uncorrelated hot spot. In contrast, in the hydrodynamic picture the two hot spots evolve and merge thus generating a larger  $v_2$  in the  $d+\text{Au}$  case. To date, no successful explanation of this detailed

geometry dependence from momentum domain calculations exists.

There are other momentum space explanations invoking color reconnection (132), radiating antennas (133), and target field anisotropy (134). Explanations invoking collectivity from interference (135) and color dipole orientation bias (136) have recently been put forward. In most of these pictures, the relation between small systems at RHIC and the LHC is ignored; the elliptic, triangular, and quadrangular flow components have no natural connection (in contrast to the case with initial geometry coupled with hydrodynamics); and the relation of  $p + p$  to  $p + A$  to  $A + A$  is ad hoc or nonexistent. Interestingly there has been a recent attempt to gauge the combined influence of initial-state momentum-domain correlations and final-state scattering (137) modeled via BAMPS. The only way to advance these alternatives is to perform comprehensive calculations across energies, geometries, and observables.

## 6. HYDRODYNAMIC DISCUSSION AND IMPLICATIONS

The modern view of hydrodynamics is as an effective theory that describes long-wavelength excitations of a system after the microscopic degrees of freedom are integrated out. The conserved charges of the theory in the simplest cases are simply the system's four-momentum components, and the equations of motion are the conservation equations  $\partial_\mu T^{\mu\nu} = 0$ , where  $T^{\mu\nu}$  is the stress-energy tensor. The fields can be taken as the fluid's four-velocity  $u^\mu$  and the energy density  $\epsilon(T)$  (or alternatively the temperature  $T$ )<sup>4</sup>. An equation of state specifying the pressure  $p = p(\epsilon)$  as a function of energy density suffices to close this simple example. However, even for an ideal fluid described by  $T_{\text{ideal}}^{\mu\nu} = (\epsilon + p)u^\mu u^\nu + pg^{\mu\nu}$  the equations of motion are clearly nonlinear due to both the form of  $T^{\mu\nu}$  and the constraint  $u_\mu u^\mu = -1$  (here we take  $c = 1$  and use the so-called mostly plus metric convention standardly used in the relativistic hydrodynamic community).

Non-ideal behavior is typically separated from the ideal fluid contribution to the stress-energy tensor:

$$T^{\mu\nu} = T_{\text{ideal}}^{\mu\nu} + \pi^{\mu\nu} \quad . \quad (3)$$

Working to first order in a derivative expansion, in the local rest frame of the fluid defined by  $u_{\text{LFR}}^\mu = (1, 0, 0, 0)$ , the spatial components of  $\pi^{\mu\nu}$  are parameterized as

$$\pi^{ij} = -\eta \left( \frac{\partial u^i}{\partial x^j} + \frac{\partial u^j}{\partial x^i} - \frac{2}{3} \delta^{ij} \partial_k u^k \right) - \zeta \partial_\mu u^\mu \quad , \quad (4)$$

where  $\eta$  and  $\zeta$  are the shear and bulk viscosities, respectively. These expressions, while perfectly consistent with the definitions of viscosity for nonrelativistic systems, lead to acausal behavior in the relativistic equation of motion. Mathematically, this is because the kernel  $\sim \exp[-x^2/(4\frac{\eta}{\epsilon+p}t)]$  is characteristic of parabolic diffusion equation; physically the superluminal behavior is encoded in the assumption that the system can react instantaneously to a shear stress.

---

<sup>4</sup>For simplicity, we assume there are no other conserved charges with associated fields.

Müller (138), then later Israel (139) and Israel-Stewart (140), developed a theory at second-order in the gradient expansion that (at the linear level) preserved causality through the introduction of a relaxation time  $\tau_{\Pi}$  for the nonequilibrium terms in the stress–energy tensor. This parameter may be viewed as a regulator for the effective theory (141) parameterizing the non-hydrodynamic (damped) modes necessary to ensure causality. As such,  $\tau_{\Pi}$  is not an unbounded free parameter, as it must satisfy  $\tau_{\Pi} > \eta/(\epsilon + p)$  to ensure that linear perturbations in the sound channel do not exceed the speed of light (142). For a given system, it is necessary to determine whether the hydrodynamic modes dominate its description or whether there is a crucial dependence on the value of  $\tau_{\Pi}$  indicating that the so-called non-hydrodynamic modes, namely the underlying physics of the regulator, are being studied (143, 144).

The necessity of the second-order term introduced by Müller-Israel-Stewart (MIS), together with the desire to apply hydrodynamics in small hadronic systems, requires understanding the order-by-order investigation of terms in the gradient expansion. The relevant expansion parameter in weakly coupled systems that admit a quasiparticle description is the Knudsen number<sup>5</sup>  $K_N \equiv \ell_{\text{mfp}}/R$ , as noted in Landau’s arguments in Section 2.

Simple estimates of parton mean free paths, under the assumption of the high parton density expected for a fully developed QGP, provided only very modest support for the validity of a hydrodynamical description in small hadronic systems:

$$\ell_{\text{mfp}} \sim (2 \text{ fm}) \left( \frac{T_0}{T} \right)^3 \left( \frac{\sigma_1}{\sigma} \right), \quad (5)$$

where  $T$  is the temperature of the plasma in MeV,  $T_0 = 200$  MeV (introduced to provide a scale; this is not the transition temperature),  $\sigma$  is the parton–parton cross section, and  $\sigma_1 = 1$  mb. Estimates such as Equation 5 have been used to argue that for collisions of large nuclei with radii  $R \sim 6\text{--}7$  fm, parton–parton cross sections no larger than a few millibarns suffice to provide mean free paths significantly smaller than the system size, ensuring  $K_N \leq 0.1$ , down to temperatures of order 200 MeV or lower.

At the same time, it is clear that even for large nuclei, the separation of scales between  $\ell_{\text{mfp}}$  and  $R$  is at best an order of magnitude. This observation leads directly to a fundamental question: What is the smallest drop of liquid QGP? Two arguments suggest that a size as small as a femtometer might be plausible. First, the successes of hydrodynamics in describing the higher moments of the flow harmonics suggested, circa 2010, that hydrodynamics was capable of describing features in the data with sizes  $\sim R/n$ , where  $n$  is the order of the flow harmonic. Second, the small value of  $\eta/s$  inferred from the data argued that the QGP must be strongly coupled, suggesting that the ballistic transport assumptions used in the above expression for the mean free paths is an overestimate. Nonetheless the observation of flow-like features in  $p + A$  and  $p + p$  collisions was a surprising development to most researchers.

---

<sup>5</sup>Again, this is a simplified description; a more general approach rooted in kinetic theory(144) allows for expansion in both  $K_N$  and the inverse Reynolds number  $\text{Re}^{-1} \sim |\pi^{\mu\nu}|/p$ , contravening Landau’s expectation that these are essentially the same in relativistic systems where hydrodynamics is applicable.

Although the MIS theory was essential in establishing the possibility of relativistic causal theory of viscous hydrodynamics, it implemented only the minimal second-order term needed to eliminate superluminal behavior. The successes of the Little Bang model described in Section 3, and the attendant interest in reliably quantifying the key parameter  $\eta/s$ , motivated efforts to systematically investigate all allowed second-order terms.

In two remarkable papers submitted (independently) to the arXiv on the same day, Baier et al. (142) and Bhattacharyya et al. (145) used the gauge/gravity duality (146,147) to not only investigate all five allowed second-order terms in a conformal theory of relativistic hydrodynamics but also calculate the magnitude of the associated transport coefficients for a strongly coupled system with the minimal value of  $\eta/s$ , in particular finding  $\tau_{\Pi} = (2 - \ln 2)/2\pi T \approx 1.31/2\pi T \approx 0.21/T$ . Romatschke (148) extended this research to the case of non-conformal hydrodynamics, in which case there are 15 second-order terms, each with an associated transport coefficient. Further efforts led to gradient expansions to all orders in linearized theory (149), and only third-order in full theory (150).

These developments led to a greatly increased understanding of relativistic hydrodynamics with important consequences for evaluating its applicability in nuclear collisions in general, and small systems in particular, in which gradients are large. There is now a vast literature on the topic, drawing insights from kinetic theory, linear response theory and the gauge/gravity duality; for thorough and masterful reviews we refer the reader to References 29 and 151. Here we summarize the important conclusions from those efforts:

1. The success of viscous relativistic hydrodynamics in describing the bulk features, in particular the  $v_n$ s, does not necessarily imply that the matter is near thermal equilibrium during its hydrodynamic evolution. Rather, it is likely that high-energy nuclear collisions remain out of equilibrium up to hadronization (31). Obviously, by definition hydrodynamics must be capable of addressing arbitrarily small perturbations about local equilibrium, but recent research has shown that this is also true in the case of momentum anisotropies of order one.
2. The key condition for the applicability of hydrodynamics in small systems is the dominance of hydrodynamics modes over non-hydrodynamic modes. This appears to be a tautological statement, but it can be put on a firm basis. Hydrodynamic modes have dispersion relations satisfying  $\lim_{|\mathbf{k}| \rightarrow 0} \omega(\mathbf{k}) = 0$  consistent with the existence of conserved charges central to the defining equations. Conversely, non-hydrodynamic modes are those with finite imaginary values of  $\omega(\mathbf{k})$  as  $\mathbf{k}$  goes to zero, indicative of transient behavior not captured in the hydrodynamic gradient expansion. Closely related to this observation is the divergence of that gradient expansion (152,153), reflecting its inability to capture the non-hydrodynamic modes. The non-hydrodynamic modes are an essential part of the early-time dynamics necessary to insure consistency and/or causality, but their late-time contributions to the dynamics should be small for hydrodynamics to apply.
3. All studies to date (29) indicate that the first two to three orders of the gradient expansion provide a very accurate description of a universal hydrodynamic attractor behavior (154)



for  $w \equiv \tau T_{\text{eff}}(\tau) > \sim 0.7$  (155), where  $\tau$  is the time from the initial collision and  $T_{\text{eff}}(\tau)$  is the effective temperature at that time as determined from the energy or entropy density. This is true even for systems that are grossly out of equilibrium, that is, have momentum anisotropies of order one.

4. These considerations have led to the concept of a hydrodynamization time,<sup>6</sup> in analogy to the (not necessarily relevant) thermalization time, and defined as the time when the hydrodynamic modes dominate the system's behavior. All indications are that this time is of order  $\tau_{\text{hydro}} \sim (0.5-1.0)[1/(T_{\text{eff}}(\tau))]$  Note that at this time first-order corrections to ideal hydrodynamics can still be large, but the subsequent evolution is well described by viscous relativistic hydrodynamics.
5. The requirement that the hydrodynamic modes dominate non-hydrodynamic effects resulting from the second-order transport coefficient  $\tau_{\Pi}$  can be used to obtain a criterion on the smallest system expected to exhibit hydrodynamic behavior. Three semi-independent lines of reasoning (109, 141, 159) led to the surprising conclusion that charged-particle rapidity densities satisfying  $dN_{\text{ch}}/dy > 2-4$  suffice for a valid description of system evolution using viscous relativistic hydrodynamics.

In summary, ample theoretical arguments developed over the past decade suggest that viscous relativistic hydrodynamics can be applied to describe particle production and flow in  $p + p$  and  $p + A$  collisions at high energies. There is strong internal consistency in this reasoning. The arguments (for the large part) rely on strong coupling, which in turn implies a small value of  $\eta/s$ , which when used in hydrodynamics modeling results in good agreement with the data. Similarly, the criterion that  $\ell_{\text{mfp}} \sim 1/T$  for minimal viscosity systems (127) is echoed in the observation (160, 161) that under these conditions a plausible bound on the minimum system size  $R$  for a hydrodynamic description is  $R \sim 1/T_{\text{eff}}$ , which is supported by numerical studies in a dual gravity system (162, 163). Further support is provided by the preservation of structure in the final state in  $A + A$  collisions up to at least  $v_5$ , which in effect are feature sizes of order one-fifth those of the nuclear size.

## 7. SUMMARY

### SUMMARY POINTS

1. Small collision systems have proved to be the perfect laboratory for studying the perfect-fluid behavior of quark-gluon plasma. As of early 2018, the field of relativistic heavy ion physics is in the midst of a revolution in our understanding of the conditions necessary

---

<sup>6</sup>In an interesting example of confluence, this awkward but accurate construct first appeared in an August 2013 paper on astrophysical plasmas (156) and in the heavy ion context in October of the same year (157) and again three weeks later (158).

for nuclear matter to behave as a near-perfect fluid with bulk dynamics described by viscous relativistic hydrodynamics.

2. The revolution has been driven by the experimental observation of flow-like features in the collisions of small hadronic systems. The theoretical insights are drawn from a broad range of studies ranging from relativistic kinetic theory to black-hole quasinormal modes in the context of the gauge/gravity duality.
3. These studies have demonstrated that the hydrodynamization time, rather than the thermalization time, is the key parameter controlling the applicability of hydrodynamics to describe the evolution of systems, and that this criterion is valid even for systems far removed from thermal equilibrium.
4. The insights derived from this ongoing work have greatly extended the regimes in which we can apply properly-formulated relativistic viscous hydrodynamics, with implications for many-body strongly coupled systems in other fields of physics.

## OPEN QUESTIONS

1. Are there alternatives to hydrodynamic modeling capable of simultaneously reproducing the experimental data from the geometry engineering of the initial state?
2. How can we understand the success of parton transport models that seemingly violate quantum mechanical limits yet reproduce flow-like features in small systems?
3. Are there experimental observables sensitive to the non-hydro modes? Can they be used to determine the associated relaxation parameters?
4. What is the smallest drop of QGP describable by relativistic viscous hydrodynamics?

## DISCLOSURE STATEMENT

The authors are not aware of any affiliations, memberships, funding, or financial holdings that might be perceived as affecting the objectivity of this review.

## ACKNOWLEDGMENTS

We are pleased to acknowledge very useful comments from Jorge Noronha, Jaki Noronha-Hostler, Constantin Loizides, Krishna Rajagopal, Paul Romatschke and Bjoern Schenke. We also acknowledge work on the graphics by Javier Orjuela-Koop. Some of the definitions that appear in the margins have been taken from the heavy ion overview article (1) that appears in this volume. JLN and WAZ gratefully acknowledge funding from the Division of Nuclear Physics of the US Department of Energy under grants DE-FG02-00ER41152 and DE-FG02-86ER40281, respectively.

## LITERATURE CITED

1. W. Busza, K. Rajagopal, and W. van der Schee, *Heavy Ion Collisions: The Big Picture, and the Big Questions*, [arXiv:1802.04801](https://arxiv.org/abs/1802.04801) [[hep-ph](https://arxiv.org/abs/1802.04801)].
2. N. Bohr, *Neutron Capture and Nuclear Constitution*, *Nature* **137** (1936) 344–348.
3. R. H. Stuewer, *The origin of the liquid-drop model and the interpretation of nuclear fission*, *Perspectives on Science* **2** (1994) 76–129.
4. N. Bohr and J. A. Wheeler, *The Mechanism of nuclear fission*, *Phys. Rev.* **56** (1939) 426–450.
5. W. Heisenberg, *Production of Meson Showers*, *Nature* **164** (1949) 65–66.
6. E. Fermi, *High-energy nuclear events*, *Prog. Theor. Phys.* **5** (1950) 570–583.
7. E. Fermi, *Collected Papers:(Note E Memorie).*, *Collected Papers* **Vol. 2** (1962) .
8. L. D. Landau, *On the multiparticle production in high-energy collisions*, *Izv. Akad. Nauk Ser. Fiz.* **17** (1953) 51–64.
9. I. Ya. Pomeranchuk, *On the theory of multiple particle production in a single collision*, *Dokl. Akad. Nauk Ser. Fiz.* **78** (1951) 889–891.

10. S. Z. Belenkij and L. D. Landau, *Hydrodynamic theory of multiple production of particles*, Nuovo Cim. Suppl. **3S10** (1956) 15. [Usp. Fiz. Nauk56,309(1955)].
11. P. Carruthers and M. Doung-van, *Rapidity and angular distributions of charged secondaries according to the hydrodynamical model of particle production*, Phys. Rev. **D8** (1973) 859–874.
12. J. D. Bjorken, *Highly Relativistic Nucleus-Nucleus Collisions: The Central Rapidity Region*, Phys. Rev. **D27** (1983) 140–151.
13. E735, T. Alexopoulos et al., *Mass identified particle production in  $p\bar{p}$  collisions at  $\sqrt{s} = 300\text{-GeV}$ ,  $540\text{-GeV}$ ,  $1000\text{-GeV}$ , and  $1800\text{-GeV}$* , Phys. Rev. **D48** (1993) 984–997.
14. MiniMax, T. C. Brooks et al., *A Search for disoriented chiral condensate at the Fermilab Tevatron*, Phys. Rev. **D61** (2000) 032003, [arXiv:hep-ex/9906026](#) [[hep-ex](#)].
15. ALICE, J. Adam et al., *Enhanced production of multi-strange hadrons in high-multiplicity proton-proton collisions*, Nature Phys. **13** (2017) 535–539, [arXiv:1606.07424](#) [[nucl-ex](#)].
16. PHENIX, K. Adcox et al., *Formation of dense partonic matter in relativistic nucleus-nucleus collisions at RHIC: Experimental evaluation by the PHENIX collaboration*, Nucl. Phys. **A757** (2005) 184–283, [arXiv:nucl-ex/0410003](#) [[nucl-ex](#)].
17. STAR, J. Adams et al., *Experimental and theoretical challenges in the search for the quark gluon plasma: The STAR Collaboration’s critical assessment of the evidence from RHIC collisions*, Nucl. Phys. **A757** (2005) 102–183, [arXiv:nucl-ex/0501009](#) [[nucl-ex](#)].
18. B. B. Back et al., *The PHOBOS perspective on discoveries at RHIC*, Nucl. Phys. **A757** (2005) 28–101, [arXiv:nucl-ex/0410022](#) [[nucl-ex](#)].
19. BRAHMS, I. Arsene et al., *Quark gluon plasma and color glass condensate at RHIC? The Perspective from the BRAHMS experiment*, Nucl. Phys. **A757** (2005) 1–27, [arXiv:nucl-ex/0410020](#) [[nucl-ex](#)].
20. P. Kovtun, D. T. Son, and A. O. Starinets, *Viscosity in strongly interacting quantum field theories from black hole physics*, Phys. Rev. Lett. **94** (2005) 111601, [arXiv:hep-th/0405231](#) [[hep-th](#)].
21. D. T. Son and A. O. Starinets, *Viscosity, Black Holes, and Quantum Field Theory*, Ann. Rev. Nucl. Part. Sci. **57** (2007) 95–118, [arXiv:0704.0240](#) [[hep-th](#)].
22. B. Muller, J. Schukraft, and B. Wyslouch, *First Results from Pb+Pb collisions at the LHC*, Ann. Rev. Nucl. Part. Sci. **62** (2012) 361–386, [arXiv:1202.3233](#) [[hep-ex](#)].
23. ALICE, J. Adam et al., *Direct photon production in Pb-Pb collisions at  $\sqrt{s_{NN}} = 2.76\text{ TeV}$* , Phys. Lett. **B754** (2016) 235–248, [arXiv:1509.07324](#) [[nucl-ex](#)].
24. P. Romatschke, *New Developments in Relativistic Viscous Hydrodynamics*, Int. J. Mod. Phys. **E19** (2010) 1–53, [arXiv:0902.3663](#) [[hep-ph](#)].
25. U. Heinz and R. Snellings, *Collective flow and viscosity in relativistic heavy-ion collisions*, Ann. Rev. Nucl. Part. Sci. **63** (2013) 123–151, [arXiv:1301.2826](#) [[nucl-th](#)].
26. S. Jeon and U. Heinz, *Introduction to Hydrodynamics*, Int. J. Mod. Phys. **E24** (2015) no. 10, 1530010, [arXiv:1503.03931](#) [[hep-ph](#)].
27. A. Jaiswal and V. Roy, *Relativistic hydrodynamics in heavy-ion collisions: general aspects and recent developments*, Adv. High Energy Phys. **2016** (2016) 9623034, [arXiv:1605.08694](#) [[nucl-th](#)].
28. H. Song, Y. Zhou, and K. Gajdosova, *Collective flow and hydrodynamics in large and small systems at the LHC*, Nucl. Sci. Tech. **28** (2017) no. 7, 99, [arXiv:1703.00670](#) [[nucl-th](#)].
29. W. Florkowski, M. P. Heller, and M. Spalinski, *New theories of relativistic hydrodynamics in the LHC era*, [arXiv:1707.02282](#) [[hep-ph](#)].
30. P. Romatschke, *Far From Equilibrium Fluid Dynamics*, [arXiv:1704.08699](#) [[hep-th](#)].
31. P. Romatschke, *Do nuclear collisions create a locally equilibrated quarkgluon plasma?*, Eur. Phys.

- J. **C77** (2017) no. 1, 21, [arXiv:1609.02820 \[nucl-th\]](#).
32. Y. Aoki, G. Endrodi, Z. Fodor, S. D. Katz, and K. K. Szabo, *The Order of the quantum chromodynamics transition predicted by the standard model of particle physics*, *Nature* **443** (2006) 675–678, [arXiv:hep-lat/0611014 \[hep-lat\]](#).
  33. Y. Aoki, S. Borsanyi, S. Durr, Z. Fodor, S. D. Katz, S. Krieg, and K. K. Szabo, *The QCD transition temperature: results with physical masses in the continuum limit II.*, *JHEP* **06** (2009) 088, [arXiv:0903.4155 \[hep-lat\]](#).
  34. F. Cooper and G. Frye, *Comment on the Single Particle Distribution in the Hydrodynamic and Statistical Thermodynamic Models of Multiparticle Production*, *Phys. Rev.* **D10** (1974) 186.
  35. H. Petersen, C. Coleman-Smith, S. A. Bass, and R. Wolpert, *Constraining the initial state granularity with bulk observables in Au+Au collisions at  $\sqrt{s_{NN}} = 200$  GeV*, *J. Phys.* **G38** (2011) 045102, [arXiv:1012.4629 \[nucl-th\]](#).
  36. J. Novak, K. Novak, S. Pratt, J. Vredevoogd, C. Coleman-Smith, and R. Wolpert, *Determining Fundamental Properties of Matter Created in Ultrarelativistic Heavy-Ion Collisions*, *Phys. Rev.* **C89** (2014) no. 3, 034917, [arXiv:1303.5769 \[nucl-th\]](#).
  37. S. Pratt, E. Sangaline, P. Sorensen, and H. Wang, *Constraining the Eq. of State of Super-Hadronic Matter from Heavy-Ion Collisions*, *Phys. Rev. Lett.* **114** (2015) 202301, [arXiv:1501.04042 \[nucl-th\]](#).
  38. J. E. Bernhard, J. S. Moreland, S. A. Bass, J. Liu, and U. Heinz, *Applying Bayesian parameter estimation to relativistic heavy-ion collisions: simultaneous characterization of the initial state and quark-gluon plasma medium*, *Phys. Rev.* **C94** (2016) no. 2, 024907, [arXiv:1605.03954 \[nucl-th\]](#).
  39. J. S. Moreland, J. E. Bernhard, W. Ke, and S. A. Bass, *Flow in small and large quark-gluon plasma droplets: the role of nucleon substructure*, in *26th International Conference on Ultrarelativistic Nucleus-Nucleus Collisions (Quark Matter 2017) Chicago, Illinois, USA, February 6-11, 2017*. 2017. [arXiv:1704.04486 \[nucl-th\]](#).  
<https://inspirehep.net/record/1591644/files/arXiv:1704.04486.pdf>.
  40. J.-Y. Ollitrault, *Anisotropy as a signature of transverse collective flow*, *Phys. Rev.* **D46** (1992) 229–245.
  41. S. Voloshin and Y. Zhang, *Flow study in relativistic nuclear collisions by Fourier expansion of Azimuthal particle distributions*, *Z. Phys.* **C70** (1996) 665–672, [arXiv:hep-ph/9407282 \[hep-ph\]](#).
  42. C. Gale, S. Jeon, B. Schenke, P. Tribedy, and R. Venugopalan, *Event-by-event anisotropic flow in heavy-ion collisions from combined Yang-Mills and viscous fluid dynamics*, *Phys. Rev. Lett.* **110** (2013) no. 1, 012302, [arXiv:1209.6330 \[nucl-th\]](#).
  43. C. Shen, U. Heinz, P. Huovinen, and H. Song, *Radial and elliptic flow in Pb+Pb collisions at the Large Hadron Collider from viscous hydrodynamic*, *Phys. Rev.* **C84** (2011) 044903, [arXiv:1105.3226 \[nucl-th\]](#).
  44. N. Borghini, P. M. Dinh, and J.-Y. Ollitrault, *A New method for measuring azimuthal distributions in nucleus-nucleus collisions*, *Phys. Rev.* **C63** (2001) 054906, [arXiv:nucl-th/0007063 \[nucl-th\]](#).
  45. M. A. Lisa, S. Pratt, R. Soltz, and U. Wiedemann, *Femtoscopy in relativistic heavy ion collisions*, *Ann. Rev. Nucl. Part. Sci.* **55** (2005) 357–402, [arXiv:nucl-ex/0505014 \[nucl-ex\]](#).
  46. D. Teaney and L. Yan, *Non linearities in the harmonic spectrum of heavy ion collisions with ideal and viscous hydrodynamics*, *Phys. Rev.* **C86** (2012) 044908, [arXiv:1206.1905 \[nucl-th\]](#).
  47. S. Pratt, *Resolving the HBT Puzzle in Relativistic Heavy Ion Collision*, *Phys. Rev. Lett.* **102** (2009) 232301, [arXiv:0811.3363 \[nucl-th\]](#).
  48. C. Shen, Z. Qiu, and U. Heinz, *Shape and flow fluctuations in ultracentral Pb + Pb collisions at*

- the energies available at the CERN Large Hadron Collider, Phys. Rev. **C92** (2015) no. 1, 014901, [arXiv:1502.04636 \[nucl-th\]](#).
49. PHENIX, A. Adare et al., *Azimuthally anisotropic emission of low-momentum direct photons in Au+Au collisions at  $\sqrt{s_{NN}} = 200$  GeV*, Phys. Rev. **C94** (2016) no. 6, 064901, [arXiv:1509.07758 \[nucl-ex\]](#).
  50. C. A. Salgado and J. P. Wessels, *ProtonLead Collisions at the CERN LHC*, Ann. Rev. Nucl. Part. Sci. **66** (2016) 449–473.
  51. K. J. Eskola, H. Paukkunen, and C. A. Salgado, *EPS09: A New Generation of NLO and LO Nuclear Parton Distribution Functions*, JHEP **04** (2009) 065, [arXiv:0902.4154 \[hep-ph\]](#).
  52. CMS, V. Khachatryan et al., *Observation of Long-Range Near-Side Angular Correlations in Proton-Proton Collisions at the LHC*, JHEP **09** (2010) 091, [arXiv:1009.4122 \[hep-ex\]](#).
  53. B. Alver and G. Roland, *Collision geometry fluctuations and triangular flow in heavy-ion collisions*, Phys. Rev. **C81** (2010) 054905, [arXiv:1003.0194 \[nucl-th\]](#). [Erratum: Phys. Rev. **C82**,039903(2010)].
  54. P. Bozek, *Collective flow in p-Pb and d-Pd collisions at TeV energies*, Phys. Rev. **C85** (2012) 014911, [arXiv:1112.0915 \[hep-ph\]](#).
  55. ATLAS, G. Aad et al., *Observation of Long-Range Elliptic Azimuthal Anisotropies in  $\sqrt{s} = 13$  and 2.76 TeV pp Collisions with the ATLAS Detector*, Phys. Rev. Lett. **116** (2016) no. 17, 172301, [arXiv:1509.04776 \[hep-ex\]](#).
  56. ALICE, B. Abelev et al., *Long-range angular correlations on the near and away side in p-Pb collisions at  $\sqrt{s_{NN}} = 5.02$  TeV*, Phys. Lett. **B719** (2013) 29–41, [arXiv:1212.2001 \[nucl-ex\]](#).
  57. ATLAS, G. Aad et al., *Observation of Associated Near-Side and Away-Side Long-Range Correlations in  $\sqrt{s_{NN}} = 5.02$  TeV Proton-Lead Collisions with the ATLAS Detector*, Phys. Rev. Lett. **110** (2013) no. 18, 182302, [arXiv:1212.5198 \[hep-ex\]](#).
  58. CMS, S. Chatrchyan et al., *Observation of long-range near-side angular correlations in proton-lead collisions at the LHC*, Phys. Lett. **B718** (2013) 795–814, [arXiv:1210.5482 \[nucl-ex\]](#).
  59. PHENIX, A. Adare et al., *Quadrupole Anisotropy in Dihadron Azimuthal Correlations in Central d+Au Collisions at  $\sqrt{s_{NN}} = 200$  GeV*, Phys. Rev. Lett. **111** (2013) no. 21, 212301, [arXiv:1303.1794 \[nucl-ex\]](#).
  60. C. Loizides, *Experimental overview on small collision systems at the LHC*, Nucl. Phys. **A956** (2016) 200–207, [arXiv:1602.09138 \[nucl-ex\]](#).
  61. R. S. Bhalerao, N. Borghini, and J. Y. Ollitrault, *Analysis of anisotropic flow with Lee-Yang zeroes*, Nucl. Phys. **A727** (2003) 373–426, [arXiv:nucl-th/0310016 \[nucl-th\]](#).
  62. N. Borghini, R. S. Bhalerao, and J. Y. Ollitrault, *Anisotropic flow from Lee-Yang zeroes: A Practical guide*, J. Phys. **G30** (2004) S1213–S1216, [arXiv:nucl-th/0402053 \[nucl-th\]](#).
  63. J.-Y. Ollitrault, A. M. Poskanzer, and S. A. Voloshin, *Effect of flow fluctuations and nonflow on elliptic flow methods*, Phys. Rev. **C80** (2009) 014904, [arXiv:0904.2315 \[nucl-ex\]](#).
  64. G. Giacalone, J. Noronha-Hostler, and J.-Y. Ollitrault, *Relative flow fluctuations as a probe of initial state fluctuations*, Phys. Rev. **C95** (2017) no. 5, 054910, [arXiv:1702.01730 \[nucl-th\]](#).
  65. ATLAS, G. Aad et al., *Measurement with the ATLAS detector of multi-particle azimuthal correlations in p+Pb collisions at  $\sqrt{s_{NN}} = 5.02$  TeV*, Phys. Lett. **B725** (2013) 60–78, [arXiv:1303.2084 \[hep-ex\]](#).
  66. CMS, S. Chatrchyan et al., *Multiplicity and transverse momentum dependence of two- and four-particle correlations in pPb and PbPb collisions*, Phys. Lett. **B724** (2013) 213–240, [arXiv:1305.0609 \[nucl-ex\]](#).

67. ALICE, B. B. Abelev et al., *Multiparticle azimuthal correlations in p -Pb and Pb-Pb collisions at the CERN Large Hadron Collider*, Phys. Rev. **C90** (2014) no. 5, 054901, [arXiv:1406.2474 \[nucl-ex\]](#).
68. CMS, V. Khachatryan et al., *Evidence for Collective Multiparticle Correlations in p-Pb Collisions*, Phys. Rev. Lett. **115** (2015) no. 1, 012301, [arXiv:1502.05382 \[nucl-ex\]](#).
69. CMS, V. Khachatryan et al., *Evidence for collectivity in pp collisions at the LHC*, Phys. Lett. **B765** (2017) 193–220, [arXiv:1606.06198 \[nucl-ex\]](#).
70. PHENIX, C. Aidala et al., *Measurements of multiparticle correlations in d+Au collisions at 200, 62.4, 39, and 19.6 GeV and p+Au collisions at 200 GeV and implications for collective behavior*, [arXiv:1707.06108 \[nucl-ex\]](#).
71. K. Dusling, M. Mace, and R. Venugopalan, *Parton model description of multiparticle azimuthal correlations in pA collisions*, [arXiv:1706.06260 \[hep-ph\]](#).
72. A. Cavagna, A. Cimarelli, I. Giardina, G. Parisi, R. Santagati, F. Stefanini, and M. Viale, *Scale-free correlations in starling flocks*, Proceedings of the National Academy of Sciences **107** (2010) no. 26, 11865–11870, <http://www.pnas.org/content/107/26/11865.full.pdf>.  
<http://www.pnas.org/content/107/26/11865.abstract>.
73. J. Jia, M. Zhou, and A. Trzupek, *Revealing long-range multiparticle collectivity in small collision systems via subevent cumulants*, Phys. Rev. **C96** (2017) no. 3, 034906, [arXiv:1701.03830 \[nucl-th\]](#).
74. PHENIX, A. Adare et al., *Centrality categorization for  $R_{p(d)+A}$  in high-energy collisions*, Phys. Rev. **C90** (2014) no. 3, 034902, [arXiv:1310.4793 \[nucl-ex\]](#).
75. J. L. Nagle, A. Adare, S. Beckman, T. Koblesky, J. Orjuela Koop, D. McGlinchey, P. Romatschke, J. Carlson, J. E. Lynn, and M. McCumber, *Exploiting Intrinsic Triangular Geometry in Relativistic He3+Au Collisions to Disentangle Medium Properties*, Phys. Rev. Lett. **113** (2014) no. 11, 112301, [arXiv:1312.4565 \[nucl-th\]](#).
76. PHENIX, A. Adare et al., *Measurement of long-range angular correlation and quadrupole anisotropy of pions and (anti)protons in central d+Au collisions at  $\sqrt{s_{NN}}=200$  GeV*, Phys. Rev. Lett. **114** (2015) no. 19, 192301, [arXiv:1404.7461 \[nucl-ex\]](#).
77. PHENIX, A. Adare et al., *Measurements of elliptic and triangular flow in high-multiplicity  $^3\text{He}+\text{Au}$  collisions at  $\sqrt{s_{NN}} = 200$  GeV*, Phys. Rev. Lett. **115** (2015) no. 14, 142301, [arXiv:1507.06273 \[nucl-ex\]](#).
78. C. Aidala et al., *Measurement of long-range angular correlations and azimuthal anisotropies in high-multiplicity p+Au collisions at  $\sqrt{s_{NN}} = 200$  GeV*, Phys. Rev. **C95** (2017) no. 3, 034910, [arXiv:1609.02894 \[nucl-ex\]](#).
79. ALICE, B. B. Abelev et al., *Long-range angular correlations of  $\pi$ , K and p in p-Pb collisions at  $\sqrt{s_{NN}} = 5.02$  TeV*, Phys. Lett. **B726** (2013) 164–177, [arXiv:1307.3237 \[nucl-ex\]](#).
80. C. Shen, J.-F. Paquet, G. S. Denicol, S. Jeon, and C. Gale, *Collectivity and electromagnetic radiation in small systems*, Phys. Rev. **C95** (2017) no. 1, 014906, [arXiv:1609.02590 \[nucl-th\]](#).
81. R. D. Weller and P. Romatschke, *One fluid to rule them all: viscous hydrodynamic description of event-by-event central p+p, p+Pb and Pb+Pb collisions at  $\sqrt{s} = 5.02$  TeV*, Phys. Lett. **B774** (2017) 351–356, [arXiv:1701.07145 \[nucl-th\]](#).
82. P. Romatschke, *Light-Heavy Ion Collisions: A window into pre-equilibrium QCD dynamics?*, Eur. Phys. J. **C75** (2015) no. 7, 305, [arXiv:1502.04745 \[nucl-th\]](#).
83. J. D. Orjuela Koop, R. Belmont, P. Yin, and J. L. Nagle, *Exploring the Beam Energy Dependence of Flow-Like Signatures in Small System d+Au Collisions*, Phys. Rev. **C93** (2016) no. 4, 044910,

- arXiv:1512.06949 [nucl-th].
84. PHENIX, C. Aidala et al., *Measurements of azimuthal anisotropy and charged-particle multiplicity in d+Au collisions at  $\sqrt{s_{NN}} = 200, 62.4, 39, \text{ and } 19.6 \text{ GeV}$* , arXiv:1708.06983 [nucl-ex].
  85. M. Gyulassy, I. Vitev, X.-N. Wang, and B.-W. Zhang, *Jet quenching and radiative energy loss in dense nuclear matter*, arXiv:nucl-th/0302077 [nucl-th].
  86. E. Norbeck, K. Afak, and P. A. Steinberg, *Hard-Scattering Results in Heavy-Ion Collisions at the LHC*, Ann. Rev. Nucl. Part. Sci. **64** (2014) 383–411.
  87. A. Accardi, F. Arleo, W. K. Brooks, D. D’Enterria, and V. Muccifora, *Parton Propagation and Fragmentation in QCD Matter*, Riv. Nuovo Cim. **32** (2010) 439–553, arXiv:0907.3534 [nucl-th].
  88. PHENIX, K. Adcox et al., *Suppression of hadrons with large transverse momentum in central Au+Au collisions at  $\sqrt{s_{NN}} = 130\text{-GeV}$* , Phys. Rev. Lett. **88** (2002) 022301, arXiv:nucl-ex/0109003 [nucl-ex].
  89. PHENIX, S. S. Adler et al., *Absence of suppression in particle production at large transverse momentum in  $S(NN)^{1/2} = 200\text{-GeV}$  d + Au collisions*, Phys. Rev. Lett. **91** (2003) 072303, arXiv:nucl-ex/0306021 [nucl-ex].
  90. STAR, J. Adams et al., *Evidence from d + Au measurements for final state suppression of high  $p(T)$  hadrons in Au+Au collisions at RHIC*, Phys. Rev. Lett. **91** (2003) 072304, arXiv:nucl-ex/0306024 [nucl-ex].
  91. BRAHMS, I. Arsene et al., *Transverse momentum spectra in Au+Au and d+Au collisions at  $s^{1/2} = 200\text{-GeV}$  and the pseudorapidity dependence of high  $p(T)$  suppression*, Phys. Rev. Lett. **91** (2003) 072305, arXiv:nucl-ex/0307003 [nucl-ex].
  92. PHOBOS, B. B. Back et al., *Centrality dependence of charged hadron transverse momentum spectra in d + Au collisions at  $S(NN)^{1/2} = 200 \text{ GeV}$* , Phys. Rev. Lett. **91** (2003) 072302, arXiv:nucl-ex/0306025 [nucl-ex].
  93. CMS, V. Khachatryan et al., *Charged-particle nuclear modification factors in PbPb and pPb collisions at  $\sqrt{s_{NN}} = 5.02 \text{ TeV}$* , JHEP **04** (2017) 039, arXiv:1611.01664 [nucl-ex].
  94. X. Zhang and J. Liao, *Jet Quenching and Its Azimuthal Anisotropy in AA and possibly High Multiplicity pA and dA Collisions*, arXiv:1311.5463 [nucl-th].
  95. C. Park, C. Shen, S. Jeon, and C. Gale, *Rapidity-dependent jet energy loss in small systems with finite-size effects and running coupling*, arXiv:1612.06754 [nucl-th].
  96. K. Tywoniuk, *Is there jet quenching in pPb?*, Nucl. Phys. **A926** (2014) 85–91.
  97. D. V. Perepelitsa, *Hard processes in small systems*, in *26th International Conference on Ultrarelativistic Nucleus-Nucleus Collisions (Quark Matter 2017) Chicago, Illinois, USA, February 6-11, 2017*. 2017. arXiv:1707.03839 [nucl-ex].  
<https://inspirehep.net/record/1609809/files/arXiv:1707.03839.pdf>.
  98. ALICE, J. Adam et al., *Centrality dependence of particle production in p-Pb collisions at  $\sqrt{s_{NN}} = 5.02 \text{ TeV}$* , Phys. Rev. **C91** (2015) no. 6, 064905, arXiv:1412.6828 [nucl-ex].
  99. ALICE, J. Adam et al., *Centrality dependence of charged jet production in pPb collisions at  $\sqrt{s_{NN}} = 5.02 \text{ TeV}$* , Eur. Phys. J. **C76** (2016) no. 5, 271, arXiv:1603.03402 [nucl-ex].
  100. ATLAS, G. Aad et al., *Measurement of long-range pseudorapidity correlations and azimuthal harmonics in  $\sqrt{s_{NN}} = 5.02 \text{ TeV}$  proton-lead collisions with the ATLAS detector*, Phys. Rev. **C90** (2014) no. 4, 044906, arXiv:1409.1792 [hep-ex].
  101. A. Adare et al., *An Upgrade Proposal from the PHENIX Collaboration*, arXiv:1501.06197 [nucl-ex].
  102. M. L. Miller, K. Reygers, S. J. Sanders, and P. Steinberg, *Glauber modeling in high energy nuclear*



- collisions*, Ann. Rev. Nucl. Part. Sci. **57** (2007) 205–243, [arXiv:nucl-ex/0701025](#) [nucl-ex].
103. K. Welsh, J. Singer, and U. W. Heinz, *Initial state fluctuations in collisions between light and heavy ions*, Phys. Rev. **C94** (2016) no. 2, 024919, [arXiv:1605.09418](#) [nucl-th].
  104. W. Broniowski, M. Rybczynski, and P. Bozek, *GLISSANDO: Glauber initial-state simulation and more...*, Comput. Phys. Commun. **180** (2009) 69–83, [arXiv:0710.5731](#) [nucl-th].
  105. J. Noronha-Hostler, J. Noronha, and M. Gyulassy, *Sensitivity of flow harmonics to subnucleon scale fluctuations in heavy ion collisions*, Phys. Rev. **C93** (2016) no. 2, 024909, [arXiv:1508.02455](#) [nucl-th].
  106. F. Gelis and B. Schenke, *Initial State Quantum Fluctuations in the Little Bang*, Ann. Rev. Nucl. Part. Sci. **66** (2016) 73–94, [arXiv:1604.00335](#) [hep-ph].
  107. B. Schenke, P. Tribedy, and R. Venugopalan, *Fluctuating Glasma initial conditions and flow in heavy ion collisions*, Phys. Rev. Lett. **108** (2012) 252301, [arXiv:1202.6646](#) [nucl-th].
  108. B. Schenke and R. Venugopalan, *Eccentric protons? Sensitivity of flow to system size and shape in p+p, p+Pb and Pb+Pb collisions*, Phys. Rev. Lett. **113** (2014) 102301, [arXiv:1405.3605](#) [nucl-th].
  109. M. Habich, G. A. Miller, P. Romatschke, and W. Xiang, *Testing hydrodynamic descriptions of p+p collisions at  $\sqrt{s} = 7$  TeV*, Eur. Phys. J. **C76** (2016) no. 7, 408, [arXiv:1512.05354](#) [nucl-th].
  110. H. Mntysaari and B. Schenke, *Evidence of strong proton shape fluctuations from incoherent diffraction*, Phys. Rev. Lett. **117** (2016) no. 5, 052301, [arXiv:1603.04349](#) [hep-ph].
  111. H. Mntysaari and B. Schenke, *Revealing proton shape fluctuations with incoherent diffraction at high energy*, Phys. Rev. **D94** (2016) no. 3, 034042, [arXiv:1607.01711](#) [hep-ph].
  112. H. Mntysaari, B. Schenke, C. Shen, and P. Tribedy, *Imprints of fluctuating proton shapes on flow in proton-lead collisions at the LHC*, Phys. Lett. **B772** (2017) 681–686, [arXiv:1705.03177](#) [nucl-th].
  113. K. Geiger and B. Muller, *Dynamics of parton cascades in highly relativistic nuclear collisions*, Nucl. Phys. **B369** (1992) 600–654.
  114. B. Zhang, *ZPC 1.0.1: A Parton cascade for ultrarelativistic heavy ion collisions*, Comput. Phys. Commun. **109** (1998) 193–206, [arXiv:nucl-th/9709009](#) [nucl-th].
  115. B. Zhang, M. Gyulassy, and C. M. Ko, *Elliptic flow from a parton cascade*, Phys. Lett. **B455** (1999) 45–48, [arXiv:nucl-th/9902016](#) [nucl-th].
  116. D. Molnar and M. Gyulassy, *New solutions to covariant nonequilibrium dynamics*, Phys. Rev. **C62** (2000) 054907, [arXiv:nucl-th/0005051](#) [nucl-th].
  117. D. Molnar and M. Gyulassy, *Saturation of elliptic flow and the transport opacity of the gluon plasma at RHIC*, Nucl. Phys. **A697** (2002) 495–520, [arXiv:nucl-th/0104073](#) [nucl-th]. [Erratum: Nucl. Phys.A703,893(2002)].
  118. D. Molnar and S. A. Voloshin, *Elliptic flow at large transverse momenta from quark coalescence*, Phys. Rev. Lett. **91** (2003) 092301, [arXiv:nucl-th/0302014](#) [nucl-th].
  119. Z. Xu and C. Greiner, *Thermalization of gluons in ultrarelativistic heavy ion collisions by including three-body interactions in a parton cascade*, Phys. Rev. **C71** (2005) 064901, [arXiv:hep-ph/0406278](#) [hep-ph].
  120. Z.-W. Lin, C. M. Ko, B.-A. Li, B. Zhang, and S. Pal, *A Multi-phase transport model for relativistic heavy ion collisions*, Phys. Rev. **C72** (2005) 064901, [arXiv:nucl-th/0411110](#) [nucl-th].
  121. Z. Xu and C. Greiner, *Shear viscosity in a gluon gas*, Phys. Rev. Lett. **100** (2008) 172301, [arXiv:0710.5719](#) [nucl-th].
  122. L. He, T. Edmonds, Z.-W. Lin, F. Liu, D. Molnar, and F. Wang, *Anisotropic parton escape is the*

- dominant source of azimuthal anisotropy in transport models*, Phys. Lett. **B753** (2016) 506–510, [arXiv:1502.05572 \[nucl-th\]](#).
123. A. Bzdak and G.-L. Ma, *Elliptic and triangular flow in p+Pb and peripheral Pb+Pb collisions from parton scatterings*, Phys. Rev. Lett. **113** (2014) no. 25, 252301, [arXiv:1406.2804 \[hep-ph\]](#).
  124. J. D. Orjuela Koop, A. Adare, D. McGlinchey, and J. L. Nagle, *Azimuthal anisotropy relative to the participant plane from a multiphase transport model in central p + Au, d + Au, and  $^3\text{He} + \text{Au}$  collisions at  $\sqrt{s_{NN}} = 200 \text{ GeV}$* , Phys. Rev. **C92** (2015) no. 5, 054903, [arXiv:1501.06880 \[nucl-ex\]](#).
  125. H. Li, L. He, Z.-W. Lin, D. Molnar, F. Wang, and W. Xie, *Origin of the mass splitting of azimuthal anisotropies in a multiphase transport model*, Phys. Rev. **C96** (2017) no. 1, 014901, [arXiv:1604.07387 \[nucl-th\]](#).
  126. L. Yan, S. Pal, and J.-Y. Ollitrault, *Nonlinear hydrodynamic response confronts LHC data*, Nucl. Phys. **A956** (2016) 340–343, [arXiv:1601.00040 \[nucl-th\]](#).
  127. P. Danielewicz and M. Gyulassy, *Dissipative Phenomena in Quark Gluon Plasmas*, Phys. Rev. **D31** (1985) 53–62.
  128. K. Dusling, W. Li, and B. Schenke, *Novel collective phenomena in high-energy proton-proton and proton-nucleus collisions*, Int. J. Mod. Phys. **E25** (2016) no. 01, 1630002, [arXiv:1509.07939 \[nucl-ex\]](#).
  129. K. Dusling and R. Venugopalan, *Azimuthal collimation of long range rapidity correlations by strong color fields in high multiplicity hadron-hadron collisions*, Phys. Rev. Lett. **108** (2012) 262001, [arXiv:1201.2658 \[hep-ph\]](#).
  130. A. Dumitru, K. Dusling, F. Gelis, J. Jalilian-Marian, T. Lappi, and R. Venugopalan, *The Ridge in proton-proton collisions at the LHC*, Phys. Lett. **B697** (2011) 21–25, [arXiv:1009.5295 \[hep-ph\]](#).
  131. B. Schenke, *Origins of collectivity in small systems*, in *26th International Conference on Ultrarelativistic Nucleus-Nucleus Collisions (Quark Matter 2017) Chicago, Illinois, USA, February 6-11, 2017*. 2017. [arXiv:1704.03914 \[nucl-th\]](#).  
<https://inspirehep.net/record/1591565/files/arXiv:1704.03914.pdf>.
  132. A. Ortiz Velasquez, P. Christiansen, E. Cuautle Flores, I. Maldonado Cervantes, and G. Pai, *Color Reconnection and Flowlike Patterns in pp Collisions*, Phys. Rev. Lett. **111** (2013) no. 4, 042001, [arXiv:1303.6326 \[hep-ph\]](#).
  133. M. Gyulassy, P. Levai, I. Vitev, and T. S. Biro, *Non-Abelian Bremsstrahlung and Azimuthal Asymmetries in High Energy p + A Reactions*, Phys. Rev. **D90** (2014) no. 5, 054025, [arXiv:1405.7825 \[hep-ph\]](#).
  134. A. Kovner and M. Lublinsky, *Angular Correlations in Gluon Production at High Energy*, Phys. Rev. **D83** (2011) 034017, [arXiv:1012.3398 \[hep-ph\]](#).
  135. B. Blok, C. D. Jkel, M. Strikman, and U. A. Wiedemann, *Collectivity from interference*, [arXiv:1708.08241 \[hep-ph\]](#).
  136. E. Iancu and A. H. Rezaeian, *Elliptic flow from color-dipole orientation in pp and pA collisions*, Phys. Rev. **D95** (2017) no. 9, 094003, [arXiv:1702.03943 \[hep-ph\]](#).
  137. M. Greif, C. Greiner, B. Schenke, S. Schlichting, and Z. Xu, *Importance of initial and final state effects for azimuthal correlations in p+Pb collisions*, [arXiv:1708.02076 \[hep-ph\]](#).
  138. I. Muller, *Zum Paradoxon der Wärmeleitungstheorie*, Z. Phys. **198** (1967) 329–344.
  139. W. Israel, *Nonstationary irreversible thermodynamics: A Causal relativistic theory*, Annals Phys. **100** (1976) 310–331.
  140. W. Israel and J. M. Stewart, *Transient relativistic thermodynamics and kinetic theory*, Annals

- Phys. **118** (1979) 341–372.
141. M. Spalinski, *Small systems and regulator dependence in relativistic hydrodynamics*, Phys. Rev. **D94** (2016) no. 8, 085002, [arXiv:1607.06381 \[nucl-th\]](#).
  142. R. Baier, P. Romatschke, D. T. Son, A. O. Starinets, and M. A. Stephanov, *Relativistic viscous hydrodynamics, conformal invariance, and holography*, JHEP **04** (2008) 100, [arXiv:0712.2451 \[hep-th\]](#).
  143. G. S. Denicol, J. Noronha, H. Niemi, and D. H. Rischke, *Origin of the Relaxation Time in Dissipative Fluid Dynamics*, Phys. Rev. **D83** (2011) 074019, [arXiv:1102.4780 \[hep-th\]](#).
  144. G. S. Denicol, H. Niemi, E. Molnar, and D. H. Rischke, *Derivation of transient relativistic fluid dynamics from the Boltzmann equation*, Phys. Rev. **D85** (2012) 114047, [arXiv:1202.4551 \[nucl-th\]](#). [Erratum: Phys. Rev.D91,no.3,039902(2015)].
  145. S. Bhattacharyya, V. E. Hubeny, S. Minwalla, and M. Rangamani, *Nonlinear Fluid Dynamics from Gravity*, JHEP **02** (2008) 045, [arXiv:0712.2456 \[hep-th\]](#).
  146. J. M. Maldacena, *The Large N limit of superconformal field theories and supergravity*, Int. J. Theor. Phys. **38** (1999) 1113–1133, [arXiv:hep-th/9711200 \[hep-th\]](#). [Adv. Theor. Math. Phys.2,231(1998)].
  147. G. T. Horowitz and J. Polchinski, *Gauge/gravity duality*, [arXiv:gr-qc/0602037 \[gr-qc\]](#).
  148. P. Romatschke, *Relativistic Viscous Fluid Dynamics and Non-Equilibrium Entropy*, Class. Quant. Grav. **27** (2010) 025006, [arXiv:0906.4787 \[hep-th\]](#).
  149. Y. Bu and M. Lublinsky, *All order linearized hydrodynamics from fluid-gravity correspondence*, Phys. Rev. **D90** (2014) no. 8, 086003, [arXiv:1406.7222 \[hep-th\]](#).
  150. S. Grozdanov and N. Kaplis, *Constructing higher-order hydrodynamics: The third order*, Phys. Rev. **D93** (2016) no. 6, 066012, [arXiv:1507.02461 \[hep-th\]](#).
  151. P. Romatschke and U. Romatschke, *Relativistic Fluid Dynamics Out of Equilibrium – Ten Years of Progress in Theory and Numerical Simulations of Nuclear Collisions*, [arXiv:1712.05815 \[nucl-th\]](#).
  152. M. P. Heller, R. A. Janik, and P. Witaszczyk, *Hydrodynamic Gradient Expansion in Gauge Theory Plasmas*, Phys. Rev. Lett. **110** (2013) no. 21, 211602, [arXiv:1302.0697 \[hep-th\]](#).
  153. A. Buchel, M. P. Heller, and J. Noronha, *Entropy Production, Hydrodynamics, and Resurgence in the Primordial Quark-Gluon Plasma from Holography*, Phys. Rev. **D94** (2016) no. 10, 106011, [arXiv:1603.05344 \[hep-th\]](#).
  154. M. P. Heller and M. Spalinski, *Hydrodynamics Beyond the Gradient Expansion: Resurgence and Resummation*, Phys. Rev. Lett. **115** (2015) no. 7, 072501, [arXiv:1503.07514 \[hep-th\]](#).
  155. M. P. Heller, R. A. Janik, and P. Witaszczyk, *The characteristics of thermalization of boost-invariant plasma from holography*, Phys. Rev. Lett. **108** (2012) 201602, [arXiv:1103.3452 \[hep-th\]](#).
  156. V. Baranov and M. Ruderman, *On the effect of transport coefficient anisotropy on the plasma flow in heliospheric interface*, Monthly Notices of the Royal Astronomical Society **434** (2013) no. 4, 3202–3207.
  157. J. Casalderrey-Solana, M. P. Heller, D. Mateos, and W. van der Schee, *From full stopping to transparency in a holographic model of heavy ion collisions*, Phys. Rev. Lett. **111** (2013) 181601, [arXiv:1305.4919 \[hep-th\]](#).
  158. P. M. Chesler, M. Lekaveckas, and K. Rajagopal, *Heavy quark energy loss far from equilibrium in a strongly coupled collision*, JHEP **10** (2013) 013, [arXiv:1306.0564 \[hep-ph\]](#).
  159. W. van der Schee, *Early hydrodynamisation, energy loss and small systems in holographic heavy*

- ion collisions*, EPJ Web Conf. **137** (2017) 07023.
160. E. Shuryak and I. Zahed, *High-multiplicity pp and pA collisions: Hydrodynamics at its edge*, Phys. Rev. **C88** (2013) no. 4, 044915, [arXiv:1301.4470 \[hep-ph\]](#).
  161. G. Baar and D. Teaney, *Scaling relation between pA and AA collisions*, Phys. Rev. **C90** (2014) no. 5, 054903, [arXiv:1312.6770 \[nucl-th\]](#).
  162. P. M. Chesler, *Colliding shock waves and hydrodynamics in small systems*, Phys. Rev. Lett. **115** (2015) no. 24, 241602, [arXiv:1506.02209 \[hep-th\]](#).
  163. P. M. Chesler, *How big are the smallest drops of quark-gluon plasma?*, JHEP **03** (2016) 146, [arXiv:1601.01583 \[hep-th\]](#).